UCRL-53220

Distant Observer Techniques for Verification of Solar Concentrator Optical Geometry

Richard L. Wood

October 30, 1981

Lawrence Livermore National Laboratory

DISCLAIMER

Work performed under the auspices of the U.S. Department of Energy by Lawrence Livermore National Laboratory under Contract W-7405-Eng-48.

UCRL-53220
Distribution Category UC-62

Distant Observer Techniques for Verification of Solar Concentrator Optical Geometry

Richard L. Wood

Manuscript Date: October 30, 1981

LAWRENCE LIVERMORE LABORATORY
University of California • Livermore, California • 94550

Available from: National Technical Information Service • U.S. Department of Commerce
5285 Port Royal Road • Springfield, VA 22161 • $6.00 per copy • (Microfiche $3.50)

CONTENTS

DISTANT OBSERVER TECHNIQUES FOR VERIFICATION OF SOLAR CONCENTRATOR OPTICAL GEOMETRY

ABSTRACT

Existing methods for testing the geometric accuracy of parabolic trough concentrators are too slow and require too much hardware and system downtime to be of use in field testing of large industrial solar installations. Distant observer techniques are developed to permit a variety of in the field tests to be made quickly and with very little equipment. The paper discusses diagnostic procedures for most correctable faults.

INTRODUCTION

If and when industry seriously begins using solar energy for industrial process heating, the parabolic trough concentrating collector is expected to make a significant contribution. The energy output at temperatures required by most industrial energy consumers makes the trough a major contender. Unlike the more familiar residential solar application, there are many candidate process heat users who are likely to need tens or hundreds of acres of collectors at each site to provide even supplemental portions of the daily energy they will require. Several small prototype systems are in use at industrial plants across the United States to test and demonstrate this technology.

Various versions of the parabolic trough concentrator are manufactured and proposed. Some are designed with relatively high concentration ratios (>60:1) to enable collection at very high temperatures (>500°F) but they require very precise construction. Others are designed for lower concentration ratios (some as low as 5:1) to relax the manufacturing tolerances and, thereby to reduce costs and to approach cost effectiveness. Of course, the energy output of these collectors at high temperatures is reduced with the reduction in concentration ratio. Performance at lower temperatures is not so badly affected, thus these cheaper collectors may be more appropriate for lower temperature applications.

Some collectors are manufactured in pieces for assembly and final adjustment at the construction site. Often the final adjustment is done by comparison to the blueprints using tape measure, plumb, templates, alignment fixtures, and, finally, intuition. Success has been varied.

Some experts say that collectors should leave the factory in nearly final form, reducing the chance of misalignment. Some say that the collector geometry should not be adjustable at all, that the structure should be rigid enough and precise enough to guarantee accuracy in assembly and operation.

Whether the collector is adjustable or not, the owner of the solar installation is likely to want some verification of correct alignment beyond the assurances of the collector manufacturer or the people in charge of installation and adjustment. For instance, if the system is not performing up to par, the investor is likely to want to know why. The system designer will blame the operators. The operators will blame the collectors. The collector manufacturer will blame the maintenance schedule. They will all blame the weather. The investor will still wonder.

Installers of parabolic trough systems and system diagnosticians need a simple, analytic method for verifying proper geometric alignment of collectors and for identifying correctable faults. Faults may be in mirror shape, both in gross misalignment, (which is correctable immediately) and in local slope errors (which are not easily correctable but effects of which can sometimes be alleviated). The large size of and investment in the proposed systems calls for a test method to be very economical in time, both in the duration of any interference with plant operation and in the lead time required to obtain complete test results.

The laser-ray trace is the only quantitative geometrical test in use thus far. Several versions of this method were developed for laboratory use to measure slope errors in collector reflectors. Sandia National Laboratory, Albuquerque, NM, has developed a semi-portable laser-ray trace apparatus which allows testing of the reflectors on operational collectors installed at their outdoor thermal test facility. None of these versions satisfy the field testing needs of large systems.

Even the semi-portable apparatus is too bulky and fragile to be easily transported. Each test run requires that the collector be held stationary and, therefore, nonproductive during the meticulous setting up and testing periods. Even then, only a relatively short section of mirror will have been

tested. The entire process must be repeated many times to test a large field. Also, only the mirror shape is tested. Receiver placement and tracker alignment must be checked in some other way.

It was noticed that the size and position of the reflected image of a receiver pipe, as seen when looking into a concentrating collector, is predictable based on assumed collector geometry and the relative position of the observer. We reasoned that the actual size and position of that image told a great deal about the actual geometry.

We obtained an example collector and began trying to analyze the images we saw. A family of test methods using this distant observer technique were developed.

The different versions being reported here have differing economic and practical advantages and disadvantages relative to one another. They share big advantages over the competing methods (blueprinting, intuition, and laser-ray tracing) in that they are analytical, require little or no system downtime, can test whole fields very quickly, require very little equipment or set up time in the field, and take a relatively short time to schedule, test, and analyze.

This paper will present the theory behind the distant observer technique, including methods of interpreting the images. Practical problems and considerations are then discussed. Finally, outlines and examples of the three specific versions of the method that we think most useful are given.

THE THEORY

A parabolic concentrating collector reflects direct sunlight onto a relatively small absorber surface called a receiver. (Rays leaving the receiver follow identical but reversed paths to the mirror and reflect back toward the sun.)

(An observer looking into the aperture of a parabolic concentrator, sees an enlarged virtual image of the receiver.) This image appears to be somewhere behind the mirror. The farther away the observer, the larger the image. When viewed from a point on the optical axis of the parabola from a great distance and when the collector is correctly configured, the image of the receiver should fill the reflector aperature completely. To account for the effective

width of the solar disk, which is not a pinpoint source, and to allow some tolerance in the tracking, drive, and support sytems, the collector also must accept rays entering within a small, finite angle from the optical axis. The aperture, therefore, should appear to be filled with the receiver image when viewed from within this same small range of off-axis angles.

Consider a parabolic trough concentrating collector with a rim angle of 90° as shown in Fig. 1. If it is configured correctly, the rays entering parallel to the optical axis (e.g., rays $\vec{S_1P}$ and $\vec{S_2E}$) are reflected to the focal point, R, via rays $\vec{PR}$ and $\vec{ER}$. Because of the finite size of the round receiver pipe, rays $\vec{H_1P}$, $\vec{L_1P}$, $\vec{H_2E}$, and $\vec{L_2E}$ also are reflected to the pipe and hit it at glancing angles. All rays which enter within the envelope of $\vec{H_2E}$ and $\vec{L_2E}$ are reflected to the pipe by the mirror element at E. It can be shown that the included angle, γ_E, is equal to the subtended angle of the receiver pipe as seen from point E,

$$\gamma_E = 2 \sin^{-1} \left(\frac{d}{2\ |ER|}\right) \approx \frac{d}{|ER|} \quad .$$

The rim is the element of the mirror farthest from the focal point. The distance from the mirror to the focal point decreases continuously as one moves along the mirror to its vertex at point B. Here, the pipe is closest to the mirror.

$$|PR| = f + \frac{p^2}{4f} \quad ,$$

where f is the focal length and p is the perpendicular distance from any point, P, to the optical axis, (see Fig. 1). p = 0 at the vertex, B, thus |BR| = f.

Likewise, the "acceptance angle," γ_p, of any point, P, on the mirror is given by

$$\gamma_p = 2 \sin^{-1} \left(\frac{d}{2\ |PR|}\right) \approx \frac{d}{|PR|} \quad .$$

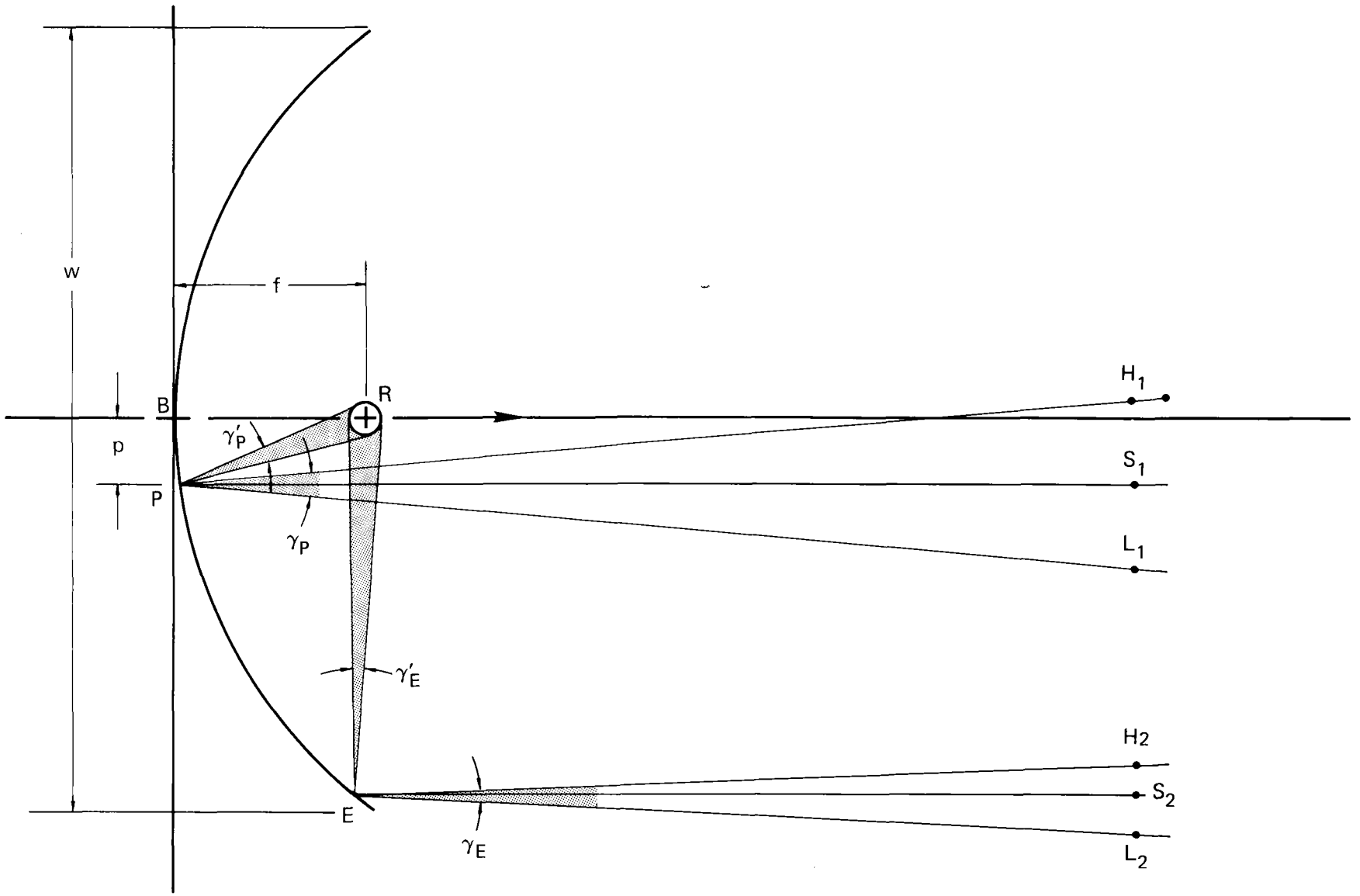

Figure 1. The acceptance angle at the edge of a parabolic concentrator mirror is significantly smaller than the acceptance angle at the center of a mirror.

For a mirror rim angle of 90°, the rim-to-focus distance, |ER|, is twice the focal length, f = |BR|. For a perfectly configured mirror with a 90° rim angle and a round receiver, therefore, the acceptance angle at the mirror's rim is only half that of the center of the mirror. The rim acceptance angle is typically in the range of 10 to 50 mrad.

Someone viewing a 6-ft-wide parabolic trough collector through a telescope at a distance of a mile or more may see a sequence of images similar to those depicted in Fig. 2. The sequence in Fig. 2a begins with an observation on the optical axis. In this case, the mirror and receiver are configured perfectly, and the entire mirror is filled with an image of the receiver. As the observer moves off the optical axis, the angle of incidence on the receiver pipe becomes more glancing. Moving to an angle, α, off the axis that is larger than half the acceptance angle of the rim, $(\gamma_E/2)$, the observer will see an image of the receiver which no longer fills the mirror aperture (see Fig. 2c). Observing farther off axis causes the image to shrink further so that only the center of the mirror is utilized (see Fig. 2d). Finally, if the observation is off axis at an angle greater than half the acceptance angle at the vertex, $(\gamma_B/2)$, the image of the receiver pipe vanishes altogether (see Fig. 2e). Any portion of the mirror not occupied by the receiver image will show a compressed, inverted view of the surroundings (e.g., earth or sky).

In Fig. 2f, the upper and lower boundaries of the graph represent the upper and lower rims of a parabolic trough. Each of the vertical lines represents one of cases a to e in Fig. 2. The horizontal spacing is indicative of the off-axis angle of each observation. The darkened area indicates the portion of the mirror which reflected the image of the receiver pipe during that observation.

If we were to plot many such observations from far away and at many points near the optical axis, we would get a graph similar to the one in Fig. 3. Each vertical bar represents one observation. For consistency, the convention used is $-\alpha$, to the left of 0 represents an observation below the optical axis, and $+\alpha$, to the right of 0, represents an observation above the axis. The horizontal band running through the center is the back (outward) side of the receiver pipe shroud seen directly by the observer.

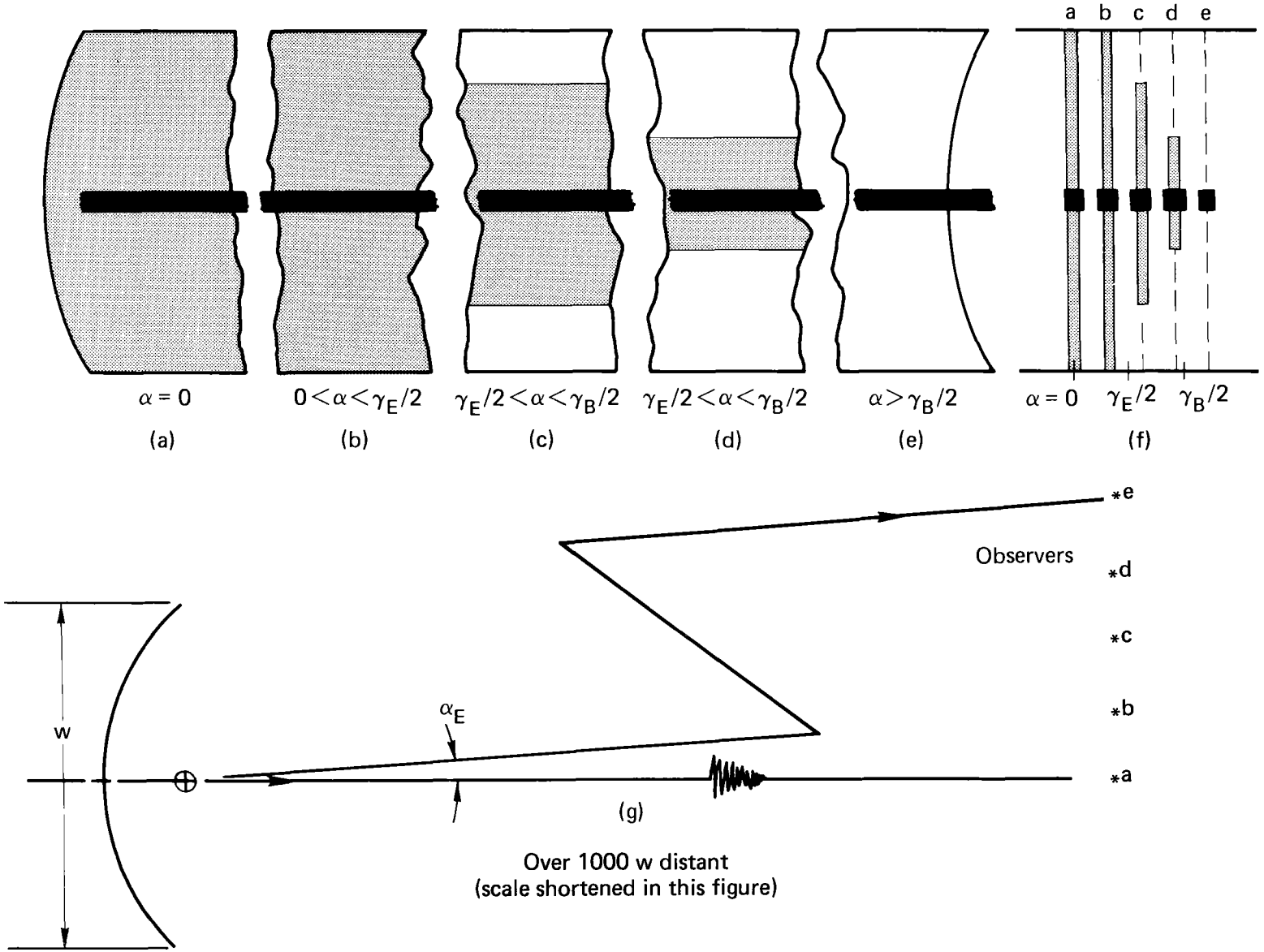

Figure 2. A sequence of images (a) to (e) reflected by a correctly configured concentrator and seen from an infinite distance by an observer moving incrementally off the optical axis as in g. The position of the images vs α, the off-axis angle is plotted in f.

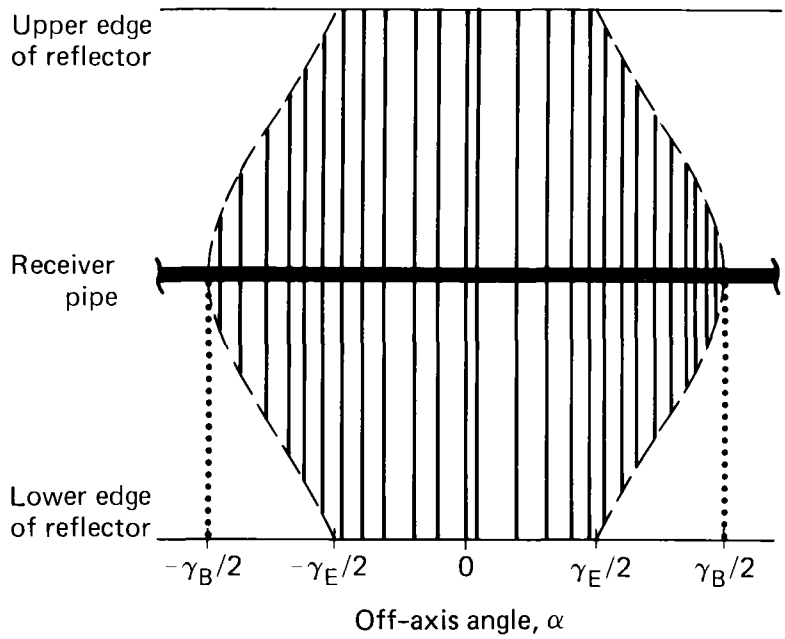

Figure 3. Plotted observations of a correctly configured concentrator produce a symmetrical pattern, that defines acceptance angles for each portion of the mirror.

In all cases, the width of the shaded region is dependent primarily upon the receiver-pipe diameter. We define the 100% acceptance band to be the widest vertical band which can fit inside this window (see Fig. 3). The 100% acceptance angle is the width of this band. All rays entering the mirror aperture within that band will be reflected to the receiver. The acceptance angle is labeled 100% because all of the mirror participates. However, the shape of the center line or bisector of the envelope tells the most about mirror shape and pipe positioning. Similar graphs can be generated to represent nonideal configurations by starting with very thin receivers to examine the effect on the shape of the bisector and then modifying these graphs to account for real pipe diameters.

Consider a trough which is not correctly configured. Assume that the mirror is correctly shaped but that the receiver is not exactly concentric with the focal point. Errors in mirror shape will be discussed later. First let us consider the trough pictured in Fig. 4. In this example, the receiver pipe still occupies the focal point, but its center is offset toward the lower edge of the trough. Again, all rays which enter parallel to the optical axis are reflected through point R. If R is internal to the pipe, all these rays strike the pipe as shown in Fig. 4.

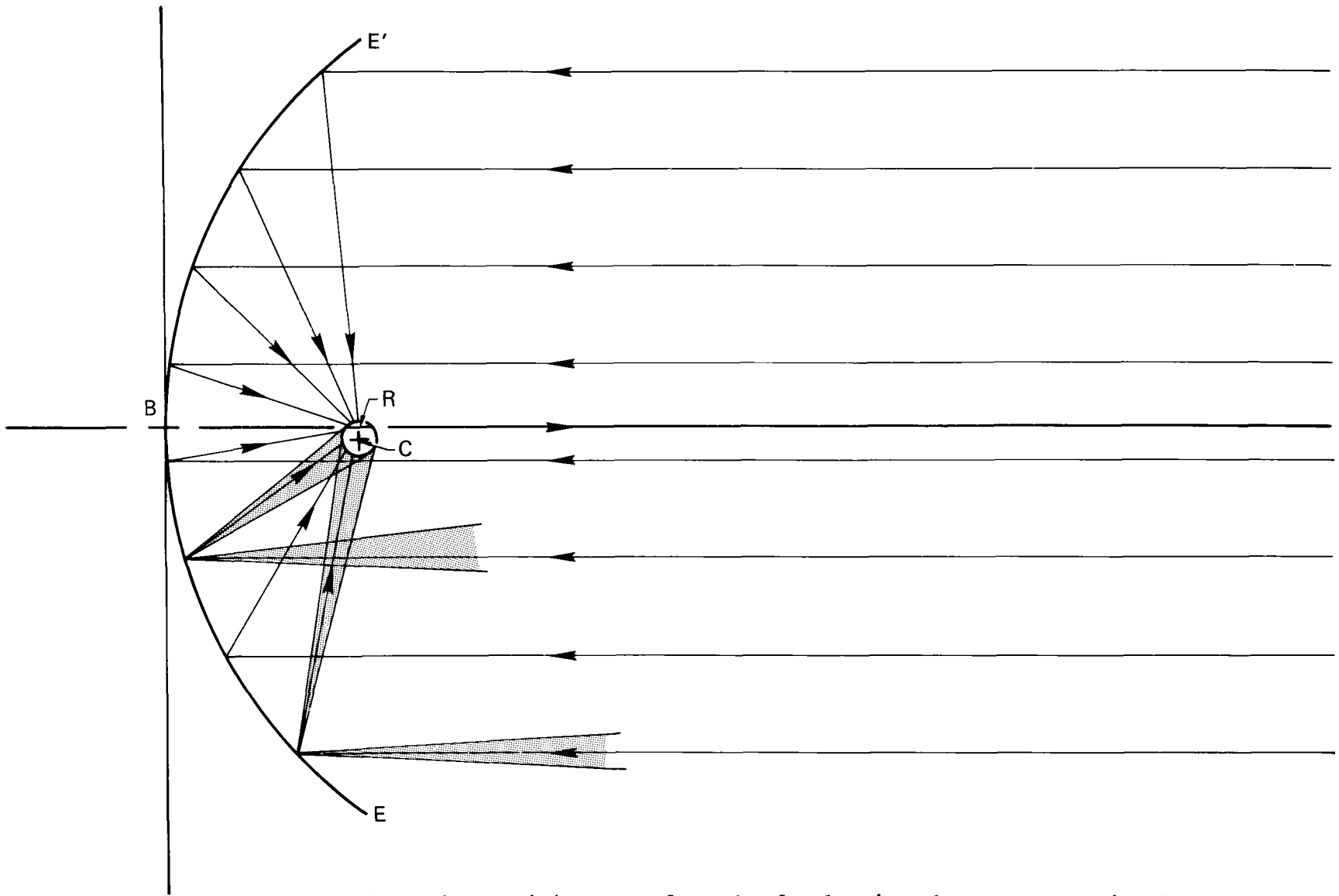

Figure 4. Shifting the receiver-pipe position away from the focal point changes to varying degrees the direction of the acceptance envelope for each part of the mirror. A lateral offset (pictured) affects the middle of the mirror more than it affects the edges.

A very narrow offset pipe would not occupy the focal point (see Fig. 5g). From a great distance an observer will see images of this pipe near the edge of the 90°-rim-angle trough only, because the pipe lies on the path of rays $\vec{ER}$ and $\vec{E'R}$ (see Fig. 5a). From a point slightly above the optical axis, $+\alpha$, the observer will see an image slightly in from each rim of the trough (see Fig. 5b). Moving further in the $+\alpha$ direction, he will see the two images move toward the center of the trough (see Fig. 5c). As the observer approaches an off-axis angle, $\alpha = \varepsilon_B \approx \frac{\mu}{f}$ the images merge (see Figure 5d). A little beyond ε_B, the image disappears (see Fig. 5e).

Figure 6 shows the effect this lateral offset would have with a realistically sized receiver in an otherwise perfect 90°-rim-angle trough. In this sequence, the receiver pipe is held at the correct distance from the mirror vertex but is progressively displaced off the optical axis toward the lower rim of the trough. Offset distances are given in fractions of receiver-pipe diameter. Offsets toward the upper rim cause identical changes but changes in the other, $-\alpha$, direction. Notice that the pipe can be offset up to about 0.25 receiver-pipe diameter without affecting the 100% acceptance band. An offset greater than 0.25 pipe diameter will reduce markedly the width of the 100% acceptance band.

Figure 7 illustrates how a 60°-rim-angle trough would be affected by a lateral offset. Again, the width of the 100% acceptance band is not affected by offsets of less than 0.25 receiver-pipe diameter, but the center of this band is shifted away from the optical axis. These collectors would perform acceptably even with offsets of up to about 0.25 receiver-pipe diameter provided their trackers were adjusted to keep the sun's relative position centered in the 100% acceptance band. For a rim angle of less than 90°, this requires pointing the tracker somewhat off the optical axis of the mirror.

Now consider misplacement of a relatively narrow receiver pipe away from the mirror, outward along the optical axis of the parabola as illustrated in Fig. 8g. In this case, an observer whose line of sight is a great distance on the optical axis will not see the pipe image near either rim because rays $\vec{ER}$ and $\vec{E'R}$ shoot under the receiver. Rays near the center of the trough however, will hit the receiver; therefore, a slightly enlarged image is seen at the center of the trough (see Fig. 8a). Figures 8b to 8e represent observations from distant points which are progressively farther above the optical axis. Images of the receiver appear only in the lower half of the mirror. From

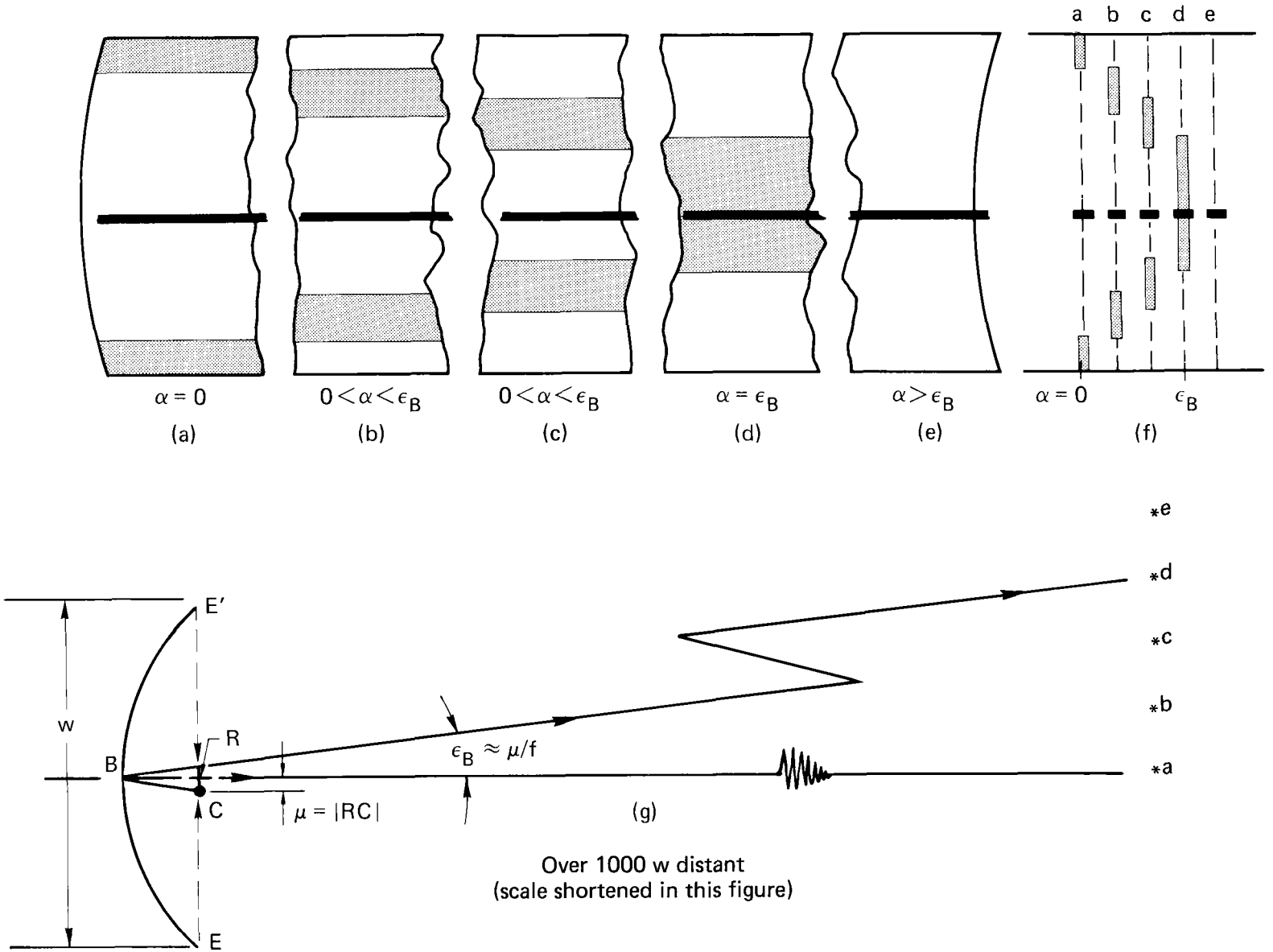

Figure 5. This sequence is similar to Fig. 2 except that the receiver pipe is offset laterally a distance, μ. Observations plotted in f show the center of the acceptance window shifted away from the optical axis by the angle $\varepsilon_B \approx \mu/f$, where f is the focal length.

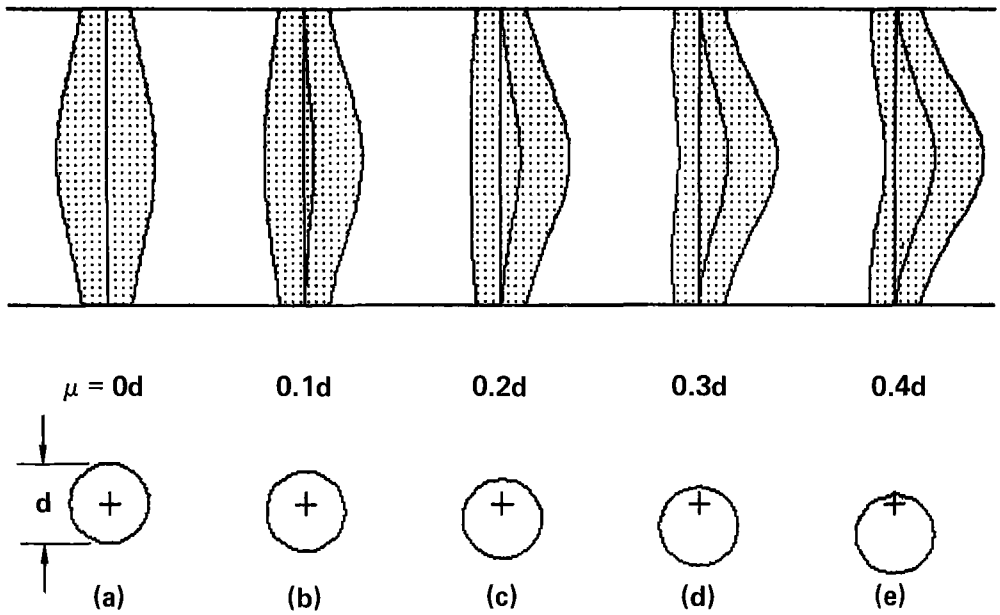

Figure 6. A family of acceptance window plots for a 90°-rim-angle mirror. The receiver pipe is offset from the focal point a distance, μ, transverse to the optical axis. The central portion of the window is bowed to one side of the optical axis.

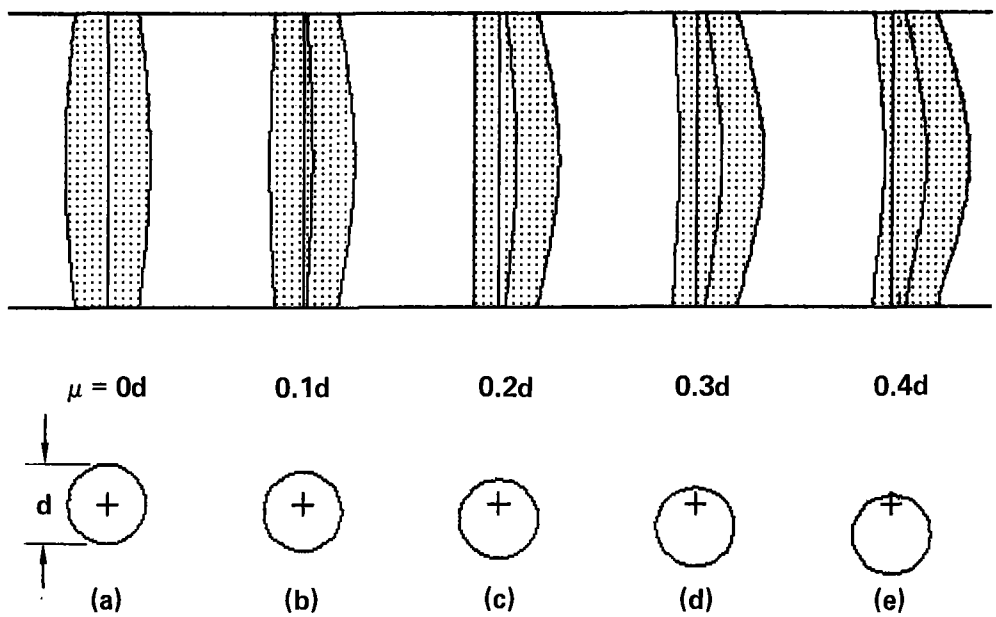

Figure 7. A family of acceptance window plots for a 60°-rim-angle mirror. The top and bottom of the window also are shifted off the optical axis.

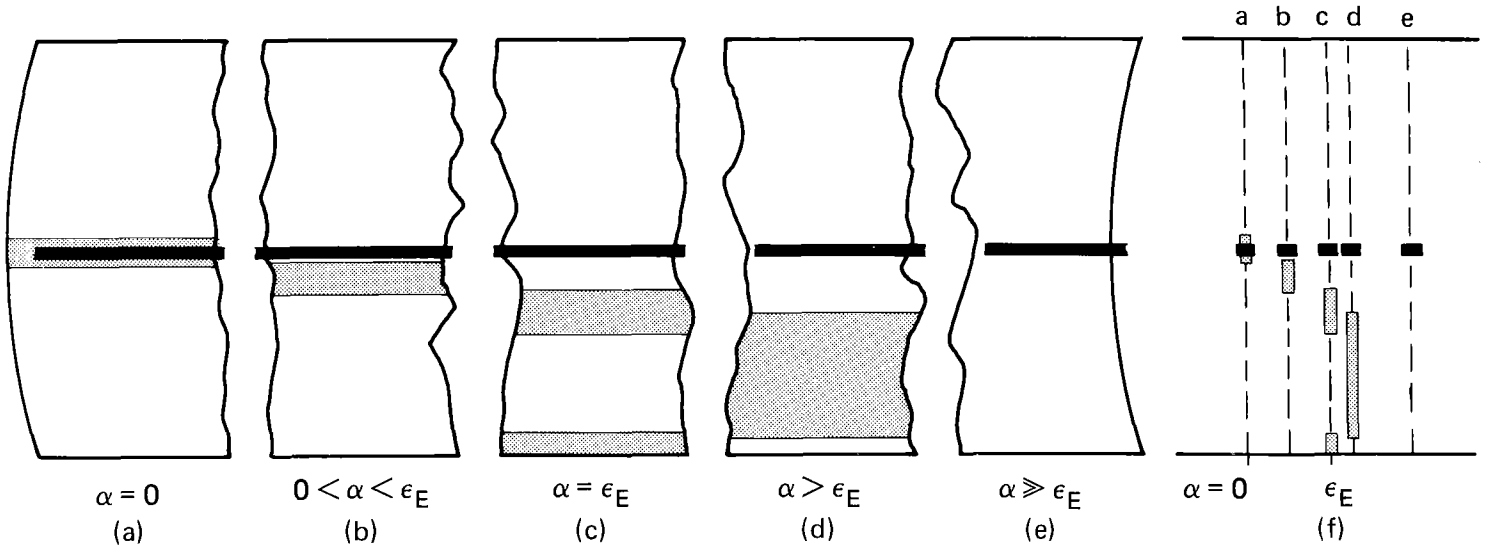

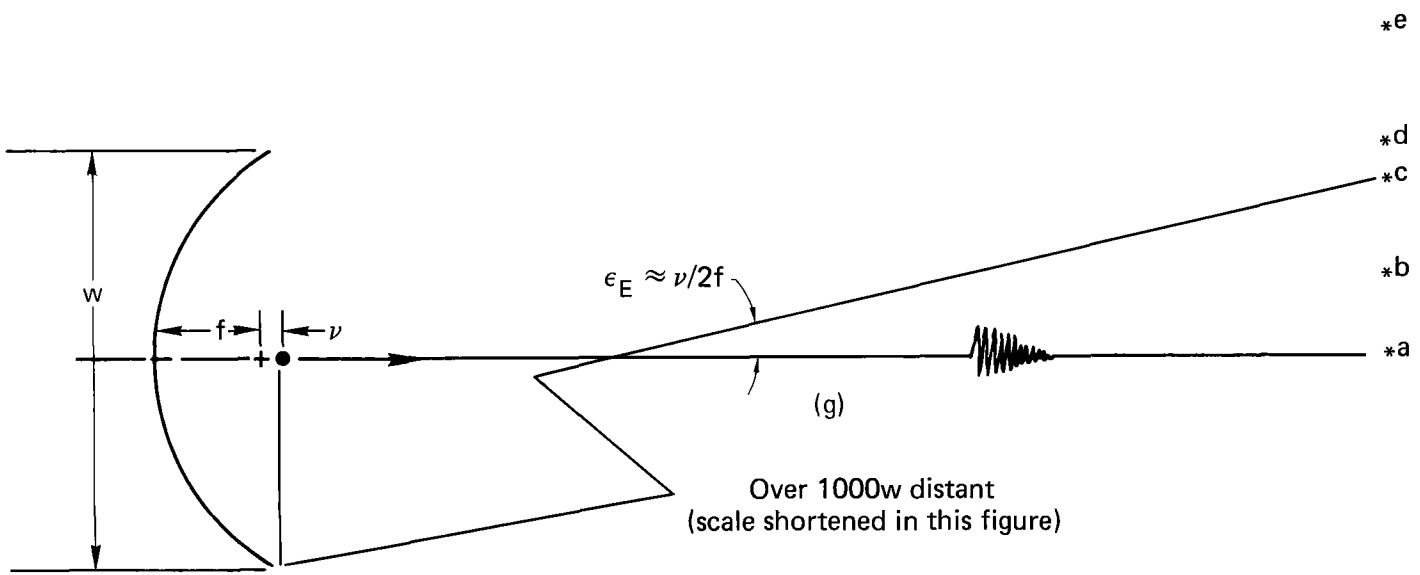

Figure 8. This sequence is similar to Fig. 2. except that the receiver pipe is displaced outward along the optical axis. From below the optical axis, $\alpha < 0$, images would appear in the upper half of the mirror.

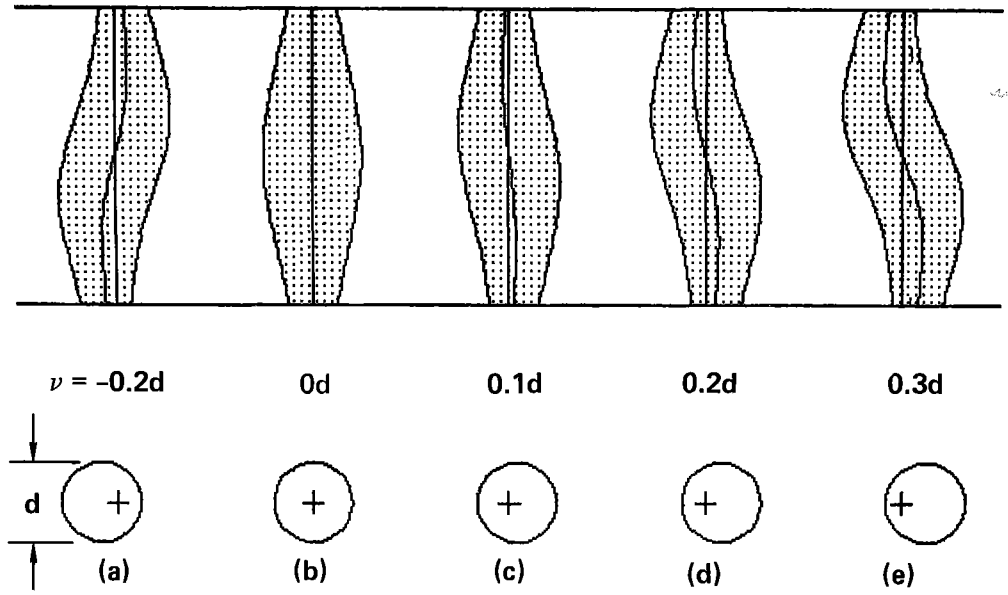

Figure 9. A family of acceptance window plots for a 90°-rim-angle mirror. The receiver pipe is displaced outward along the optical axis a distance, ν. The position of the central point is unaffected, but the ends are moved off the optical axis by the angle $\epsilon_E \approx \nu/2f$.

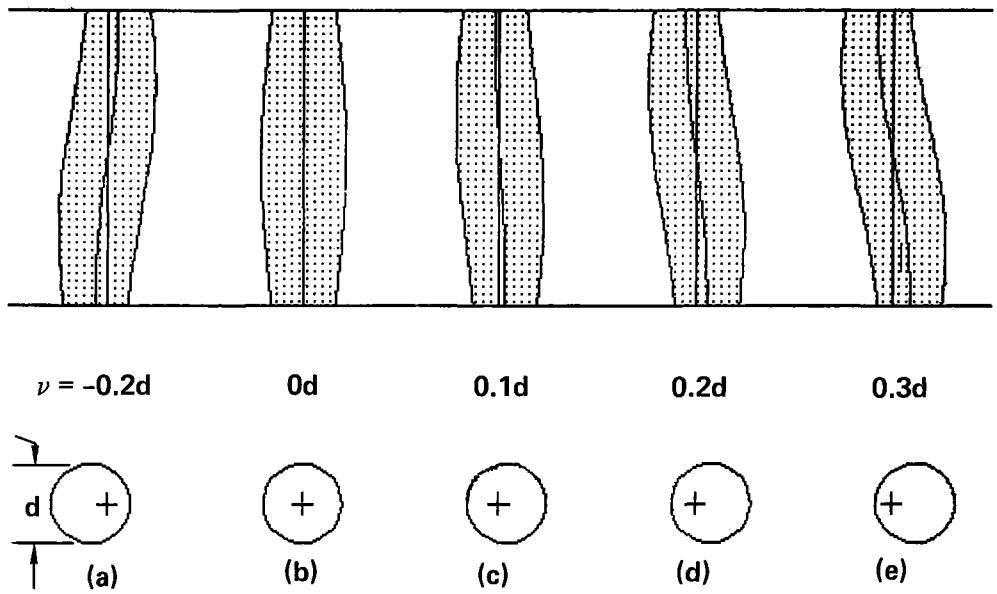

Figure 10. A family of acceptance window plots for a 60°-rim-angle mirror. The receiver pipe is displaced outward along the optical a distance, ν.

below the optical axis, the images would appear in the upper half of the mirror only.

Figure 9 illustrates the effect of misplacement of a realistically sized receiver pipe into or out of the mirror trough. In this sequence, the receiver pipe is kept centered on the optical axis but is moved progressively outward along the axis, starting nearer than the true focal point and ending beyond it. Again, distances are given in fraction of receiver diameter. An S-shaped acceptance pattern results from the pipe being too far from the mirror, a backwards S-shaped pattern results from the pipe being too close. Figure 10 illustrates the same effect on a 60°-rim-angle collector. Notice that in either case, even a small error in either direction in the receiver-to-mirror vertex distance causes a marked decrease in the 100% acceptance angle. The pattern is still centered on the optical axis, thus readjustment of the tracker cannot nullify the problem.

Some parabolic trough collectors have adjustable mirror segments. A common arrangement is to hinge the mirror along its vertex. Should the mirrors be set at the wrong angles, the resulting acceptance patterns for the two halves should be analyzed separately. Figures 11a to 11e show the predicted patterns for a collector with both the upper and lower halves of the mirror rotated outward by an angle, ϕ. Notice that the 100% acceptance band is markedly affected. This can be greatly alleviated by repositioning the receiver pipe outward, a distance $\Delta v \approx 2\phi f$ (see Figs. 11f to 11j).

The results of simultaneous lateral and axial errors in receiver pipe position are illustrated in Fig. 13. Only one quadrant is shown, but the other three have similar patterns with left and right and/or up and down directions reversed.

We have shown what an observer would see in a parabolic concentrator from a distance >1000 apertures (w) and have explained a little about how to interpret the reflected images. In practice, it is seldom easy to find a vantage point that far away. We will show that an observer can gather the same data from a point much closer to the concentrator.

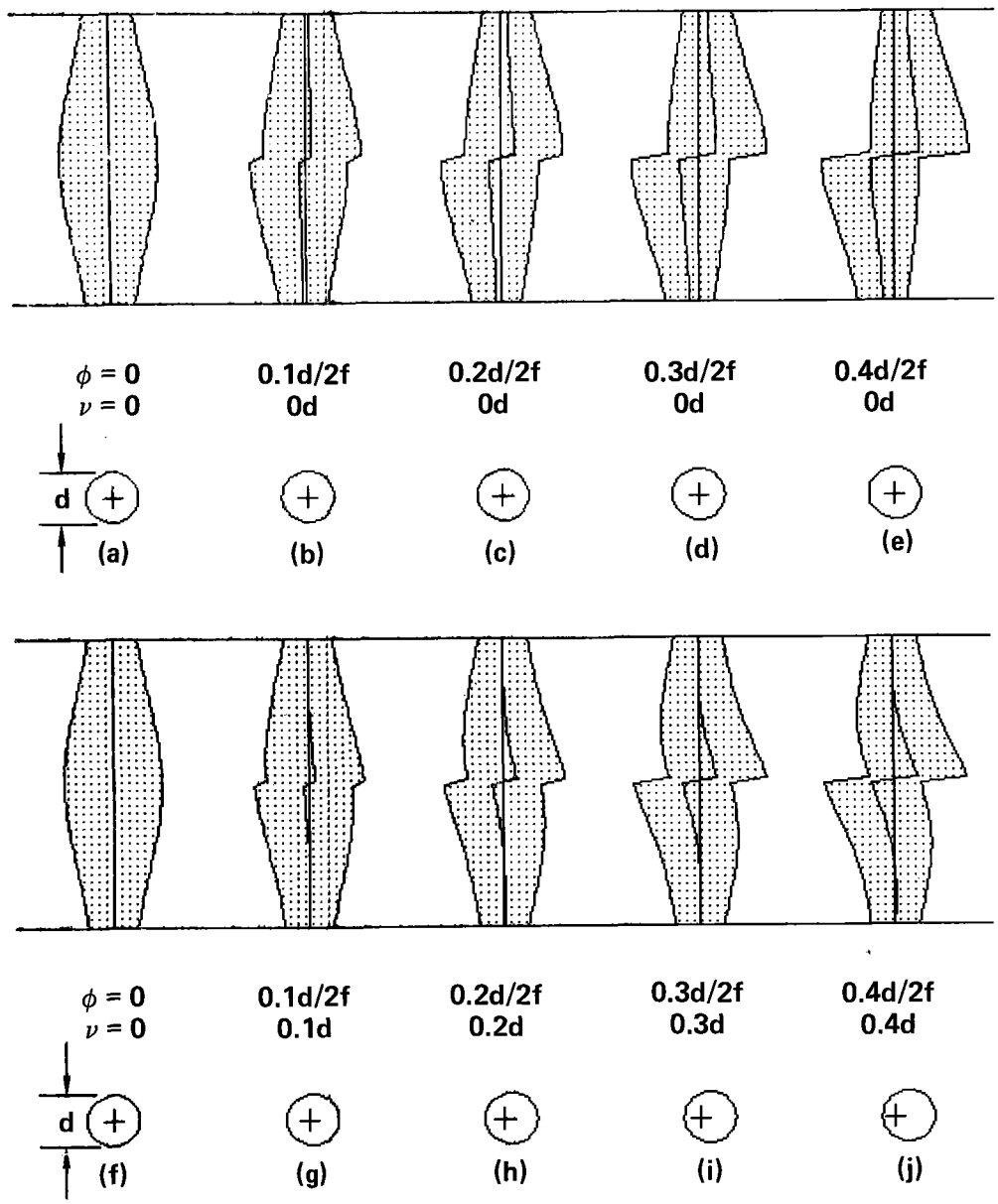

Figure 11. Two families of acceptance-window plots for a nominal 90°-rim-angle mirror with adjustable mirror halves. Both the mirror halves are pivoted away from the receiver pipe by an angle, ϕ. In (a) to (e), the pipe is fixed at the nominal focal point, a distance, f, from the vertices of both halves. In (f) to (j), the pipe is moved outward a distance, $d = 2\phi f$, to shift top and bottom of the window back to the nominal optical axis, $\alpha = 0$.

Assume that the mirror and receiver are perfectly configured. In Fig. 12, the observer at point S sees an enlarged virtual image of the receiver in the mirror.

We plot this view on the same width vs α grid as before, but because the observer cannot be considered infinitely distant, he is at a different off-axis angle for every point across the opening. Ray $\overrightarrow{CS}$ is parallel to the

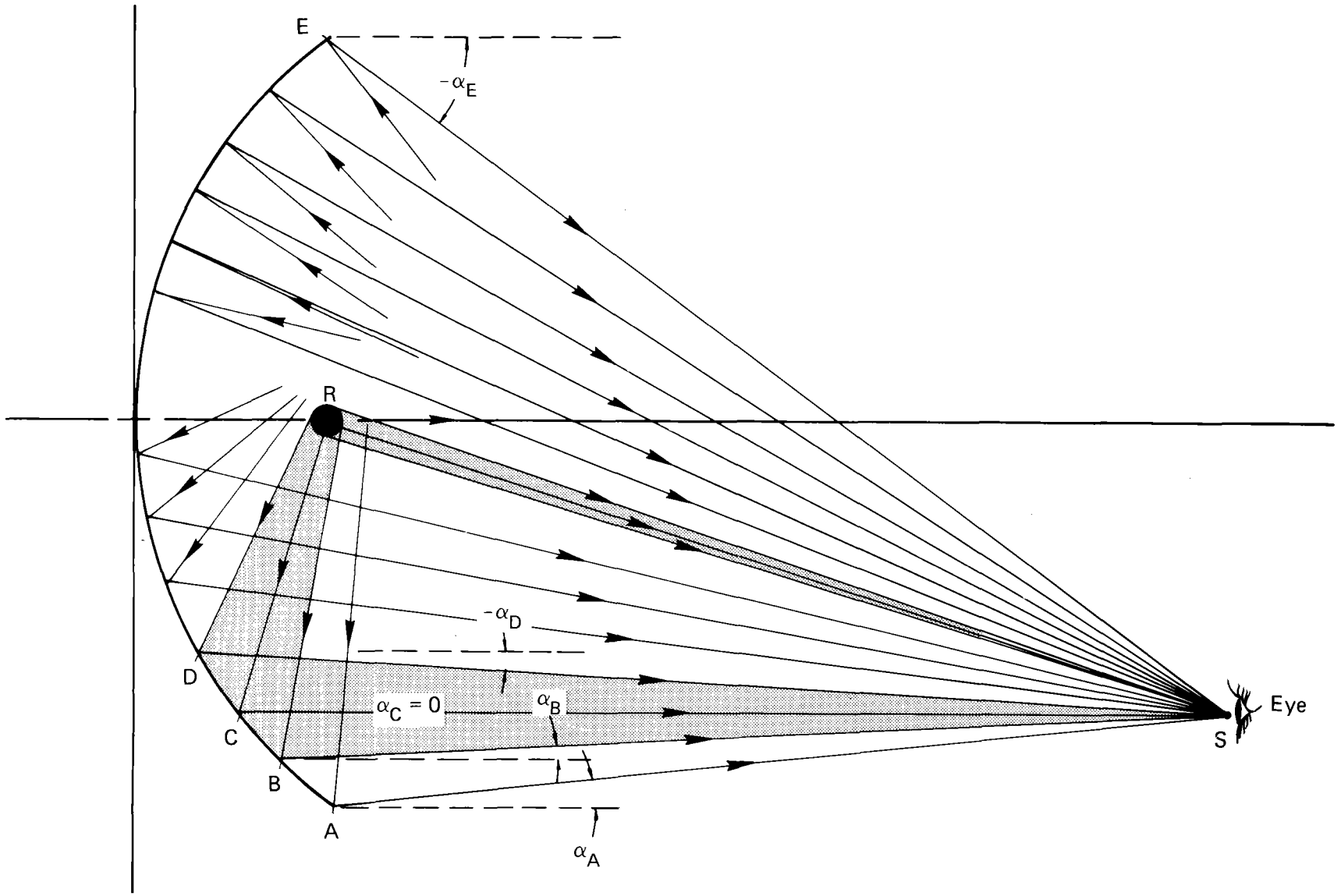

Figure 12. In an observation from any point, S, that is a practical distance from the concentrator, each point, P, on the mirror is seen at a different angle from the optical axis, α_P.

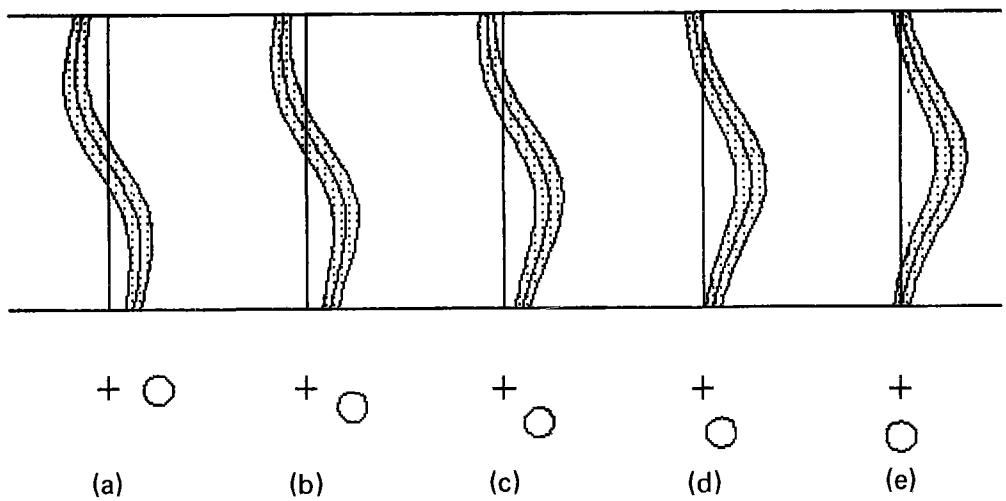

Figure 13. A family of acceptance window plots for a 90°-rim-angle mirror. In (a) through (e), the receiver pipe is off center the same total distance. In (a), there is no lateral offset; all the error is along the optical axis. In (e), all the error is in the lateral direction.

optical axis, $\alpha = 0$, thus the image is seen behind point C on the mirror. Ray $\vec{AS}$ is pointed up at an angle α_A. An observer at a great distance from and above the optical axis by α_A would have seen the same thing at point A. Similarly, ray $\vec{ES}$ is aimed at a very distant point below the optical axis at an angle $-\alpha_E$. Likewise, every point on the mirror is observed at a different off-axis angle α. If the observer is at least 5w away, the variation in α is approximately linear with distance across the opening, and perspective effects can still be ignored. This parallax error must be accounted for when plotting observation data.

Figure 14 illustrates the many observations made as the now-not-so-distant observer moves from well below the optical axis, $-\alpha$, to well above it, $+\alpha$. This concentrator, as in Fig. 2, is perfectly configured. In Fig. 14f, these observations are plotted with the proper parallax adjustments. By adding more observations, an envelope can be generated identical to the one in Fig. 3.

Thus far, we have examined the effects of receiver-pipe misplacements in perfectly shaped parabolic mirrors, however, mirror-slope error also must be considered. Others have done extensive work in developing ways of measuring mirror-slope errors in real collectors. These methods are used as laboratory procedures to check manufacturing tolerances, and are not conducive to field testing. As we will further illustrate, mirror-slope errors can often be alleviated by appropriate receiver-pipe positioning. Since these competing test methods do not sense the receiver pipe optical position, such fixes are not made possible.

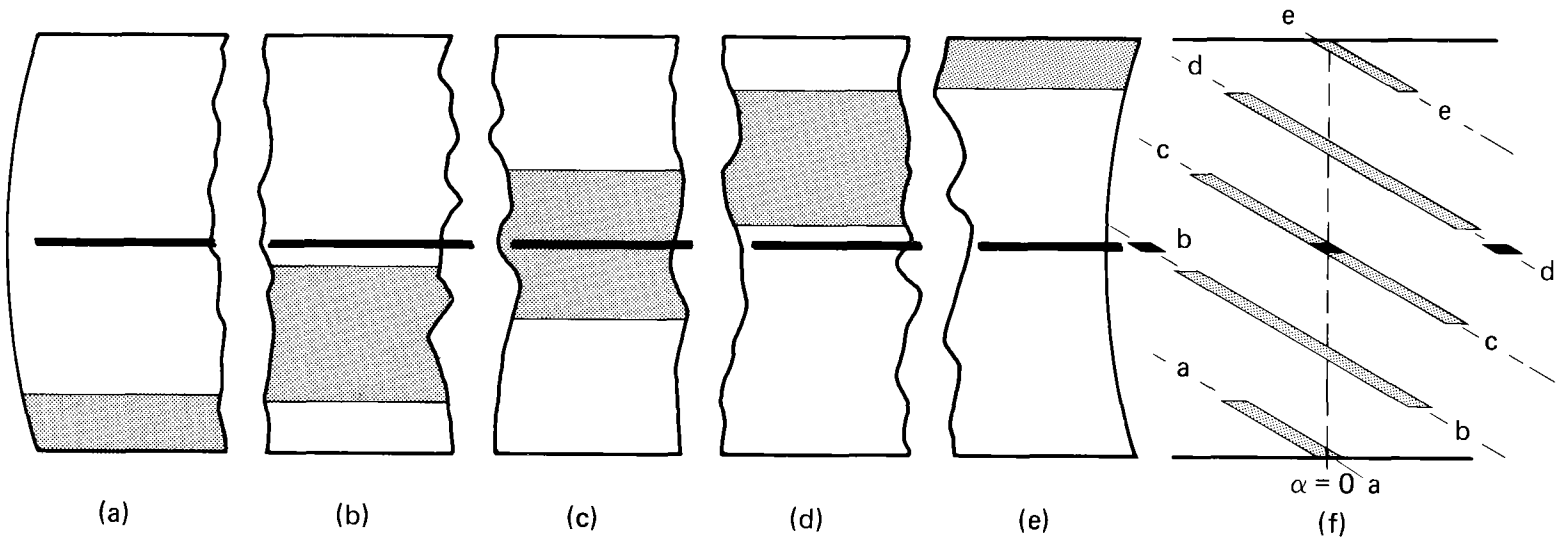

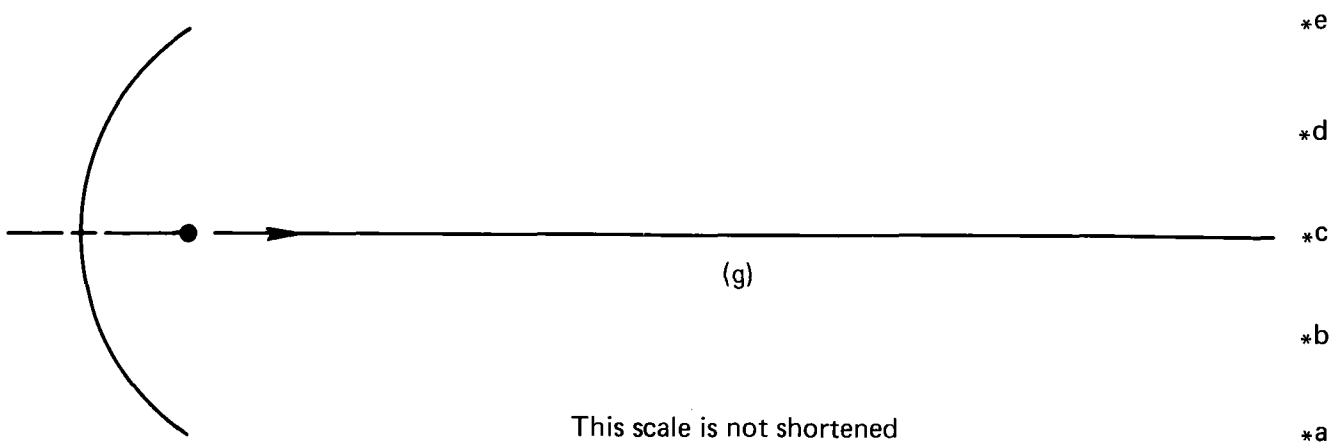

Figure 14. A sequence of images (a) to (e) seen by an observer at a practical distance. The images move incrementally from below the optical axis to above it. The position of the images vs α, the off-axis angle, is plotted in (f), taking into account the variation in α within each observation.

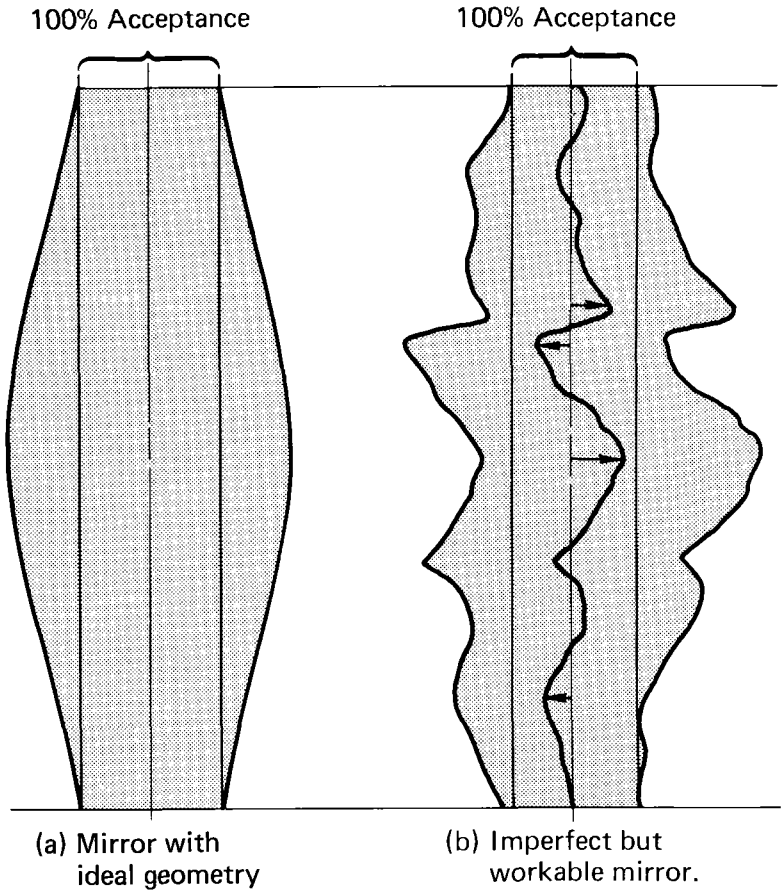

Figure 15. All manufactured collector-mirrors have some waviness that affects the shape of the acceptance window. The mirror slope error at any point on the mirror is the distance from the window-bisecting curve to the vertical line at $\alpha = 0$.

Figure 15, illustrates the acceptance windows of two collectors. The first collector (see Fig. 15a) has a perfectly shaped parabolic mirror with a perfectly positioned receiver. The second plot (see Fig. 15b) represents a more realistic case. Thus, the acceptance window is more complex with all the waviness present in real mirrors. In this plot, the dark borders of the window are defined by the edges of the receiver images, as seen in the many observations. A dark curved line bisects the window. At any point on the mirror, the mirror-slope error is given directly by the deviation of this bisecting curve from the ideal vertical straight line at that point, and is indicated by the four small arrows in the figure.

THE PRACTICE: MAKING, RECORDING AND INTERPRETING OBSERVATIONS

Several choices exist for the observation procedure and recording medium. These choices will affect the accuracy and completeness of the data as well as the ease of interpretation and the cost of performing the test.

In designing a test the most important considerations are:

1. What is to be proved or discovered, i.e., a precise determination of the mirror slope error or a check of the gross pipe positioning?
2. How large is the field to be tested?

Other considerations are: Collector accessibility, cost and availability of test equipment, urgency of results, system downtime and other conflicts or interruptions in plant operations or personnel.

The variables that define the test scheme are:

1. The number and angular spacing of observations to be made per test cross section, as well as the number and spacing of test cross sections per collector. Some method for measuring the angular change between observations must be defined.
2. The recording medium. The methods we have used are memory, sketches, and photos. Video is a conceivable (if elaborate) alternative that could speed data reduction and interpretation, particularly if it were tied to equally elaborate digital equipment and software. A specially designed strip camera has been proposed, which would directly yield photographs of the acceptance pattern, eliminating several data reduction steps.
3. The distant vantage point. Within the resolution limits of the viewing apparatus, the farther away the observer, the better. Accuracy of results is diminished if the observer is closer than approximately ten times the aperture width. This distance, L, must be measured to adjust for parallax. At close range, the accuracy requirement is tight (for $L \approx 10$ w, an error of ± 0.2 w, or 2%, yields an error of 2 mrad); whereas at great range it is less critical (for $L \approx 100$ w, an error of +25 w to -17 w (or ~20%) yields, an error of 2 mrad). If the observer is farther than ~500 w away, no parallax adjustment seems necessary. In multiple row arrays, only the front rows can be seen from ground level. An elevated vantage point is needed to view the interior rows; e.g., rooftops, balconies, scaffolds, lampposts, high-lift trucks, or aircraft.

The following discussion presents some useful schemes and the advantages of each will be discussed. Combinations of recording frequency, recording medium, and vantage point other than those discussed here may be appropriate in certain situations for various requirements.

SCHEME A: STATIONARY OBSERVER AT AN INTERMEDIATE DISTANCE

The sequence of photos of the test collector shown in Fig. 16 frames 1 to 63 was taken from the top of a lift truck at a distance of about 50 ft (~15 m or ~15 focal lengths). The relative motion of the observer with respect to the optical axis was done by rotating the collector with its tracking motor.

The receiver image does not fill the aperture in any of the frames at this range. From this elevated vantage point, the sky makes up the major portion of the background against which the receiver image is seen. Both the ground behind the truck and the truck are reflected in the extreme upper part of the mirror. A short sequence taken from ground level appears in Figs. 16x to 16z. The earth background is seen to fill the entire upper half of the mirror. There is not enough contrast between the receiver and the ground to show an edge using black and white film; however, the edge can be distinguished on color film. These photos were taken before 10 am to avoid having the sun's image reflect in the mirror. At 15 m distance (~15 focal lengths) there is no danger to the observer from solar concentration, but the reflection of the bright sun in the background sky washes out the picture.

To indicate collector rotation, a red and yellow checkerboard pattern was affixed to the mirror prior to shooting the film. It took 6 seconds to film the whole sequence of photos using a 35-mm-motion-picture camera set at 16 fps. During the filming, the collector moved at a constant speed from the tracking position to the stowed position using the normal tracking gear and motor. The angular change per frame can be calculated easily, assuming the rate is constant, by counting the number of checkerboard lines passed by the receiver pipe in a given number of frames and knowing the spacing of the lines and its distance from the pipe.

Variations in the image pattern are quite apparent along the length of the trough. This obvious longitudinal nonuniformity is small when compared to the overall shape of the assembly. We will analyze the collector shape at the four cross sectional planes indicated in Fig. 17.

A convenient way to compile the photographic data is to display each frame on a tablet and to measure the image position with a scale. This is a tedious task if done manually. There are several commercially available devices equipped with film projectors that make the process much easier and more reliable. These projection devices have a tablet or screen with a pointer or cursor that can be moved to any point on the tablet or screen. The

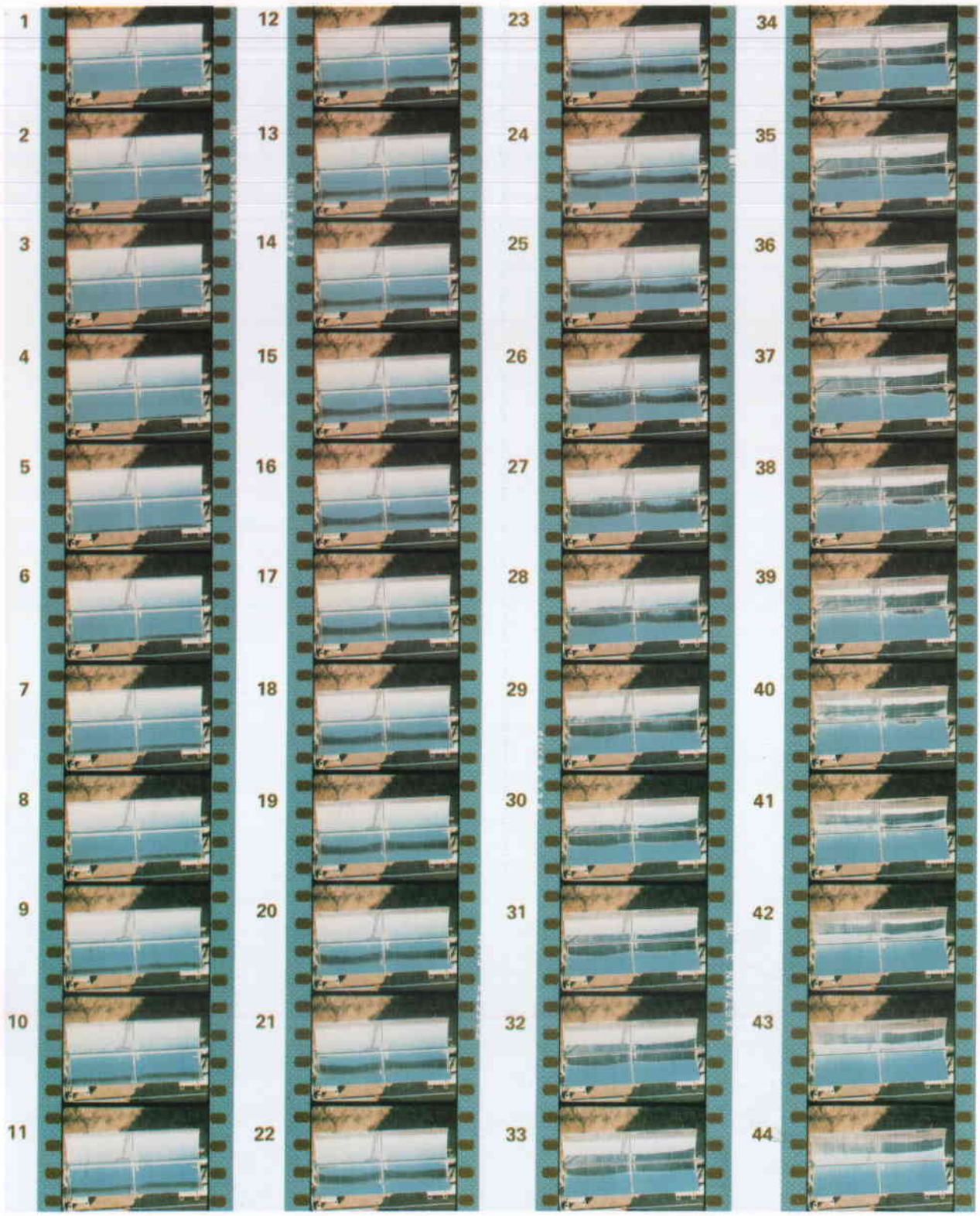

Figure 16. Motion picture film of a test collector with tracking motor activated. Data from the frame count and the red/yellow checkerboard protractor indicates that the angular change taking place between one frame and the next is 3.48 mrad (~0.199°).

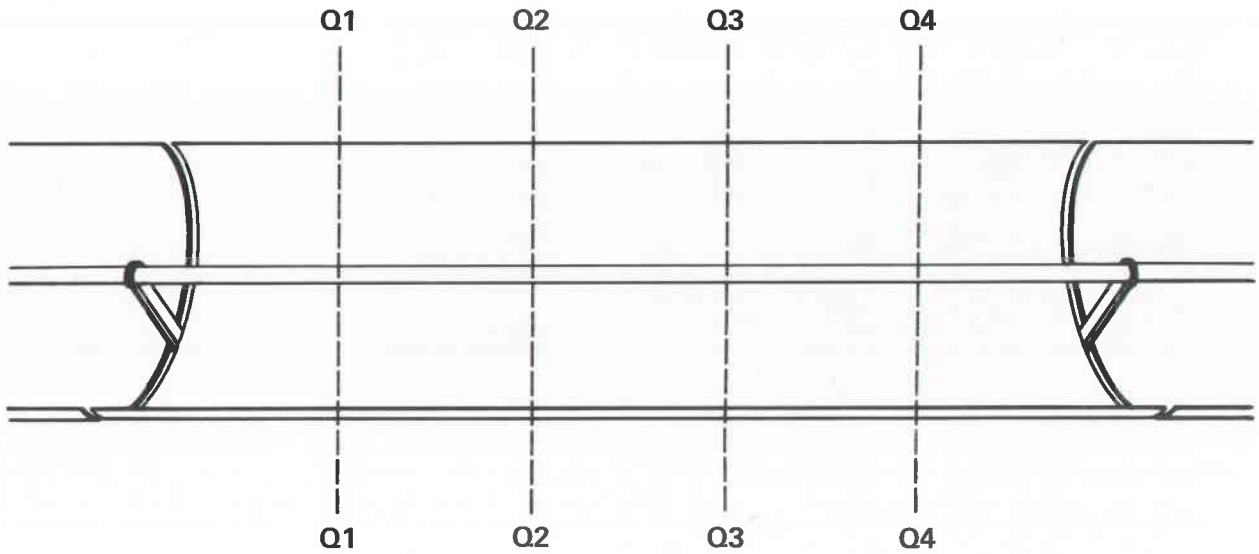

Figure 17. Acceptance window plots are made each for a particular cross sectional cut of the collector. In these tests we analyzed the observations at four places along its length, Q1, Q2, Q3, and Q4.

coordinate position of the cursor is sensed mechanically or electronically, and the locations of the points of interest recorded and reported automatically using punched cards, tape, or electronic media.

At LLNL we used such a device. The data was fed into a minicomputer that also plotted the acceptance patterns. While the owner of an industrial solar collector may not wish to purchase such elaborate testing equipment, an independent testing laboratory may find it cost effective.

We proved the validity of this method by observing a section of a test collector at LLNL. The collector was adjustable in several ways to impose various faults on its shape. The reflector's upper and lower halves were supported independently with a hinge joint along the vertex and with movable outer support-screws and locking jam-nuts. The mirrors were quite flexible, permitting local distortions if desired. Also the receiver position was adjustable.

We asked a technician aided by a sunny day and armed with only a set of wrenches, a tape measure, and a set of blueprints, to adjust our newly assembled collector. Afterwards, the aforementioned 35-mm motion picture was made of the collector as it rotated past our position atop a 50-ft lift platform (see Fig. 16). The image positions on each frame were measured and recorded using the projection device. Measurements of the trough width, observer-to-collector distance, and receiver-to-checkerboard distance were

used to calculate both the angle that the trough had rotated from one frame to the next and the subtended angle of the aperture from the observation point. These angles determine the spacing between and the parallax angle of the observation lines in the acceptance plot. Refer to the discussion of Figs. 13 and 14 for an explanation of the procedure.

The acceptance plots shown in Fig. 18 were made from this data. The scale across the bottom is in milliradians (mrad) and is a relative scale (i.e., 0 mrad corresponds to the center point on the first frame digitized, which is a relatively arbitrary point). The waviness of the mirror segments is apparent. Closer examination shows that coverage of the aperture between the 35 and the 40 mrad grid lines is fairly complete.

Using the principles laid out in earlier sections, it is possible to manipulate the data to predict the effects of various collector adjustments on the shape of the acceptance envelopes. We programmed the governing relationships into the plotting routine to allow us to do this interactively on the computer.

The crude S-shape of the envelopes might suggest that the pipe is too far out of the trough. Before coming to this conclusion, notice that this trough is slightly narrower than three times its focal length and has an ~72° rim. Compare these envelopes with the shapes in Fig. 9. Pipe displacement outward along the optical axis causes the upper endpoint of the envelope to shift to the left. In the observed data the endpoints are close to center. Fig. 19 shows the effect that an axial adjustment into the trough would have on the envelope for the first quarter cross section. As expected, the upper endpoint is shifted to the right, and the 100% acceptance window is reduced.

The marked S-shape seen in this data is a consequence of the independent adjustability of the upper and lower mirror halves. They were set too far inward. Thus, the pattern in either half looks like the pipe was offset in that direction. Figure 20 illustrates the effect of rotating the mirrors outward.

The patterns in Fig. 21 were arrived at after several trials. The 40-mrad grid line in this data set seemed to be closest to the centroid; therefore, an attempt was made to get the widest possible 100% acceptance bands centered about this line for each of the four cross sections. It is important to aim all parts of the collector in the same direction. Table 1 summarizes those adjustments necessary to obtain these results. In spite of the very apparent slope errors in the mirrors, it may be possible to get a

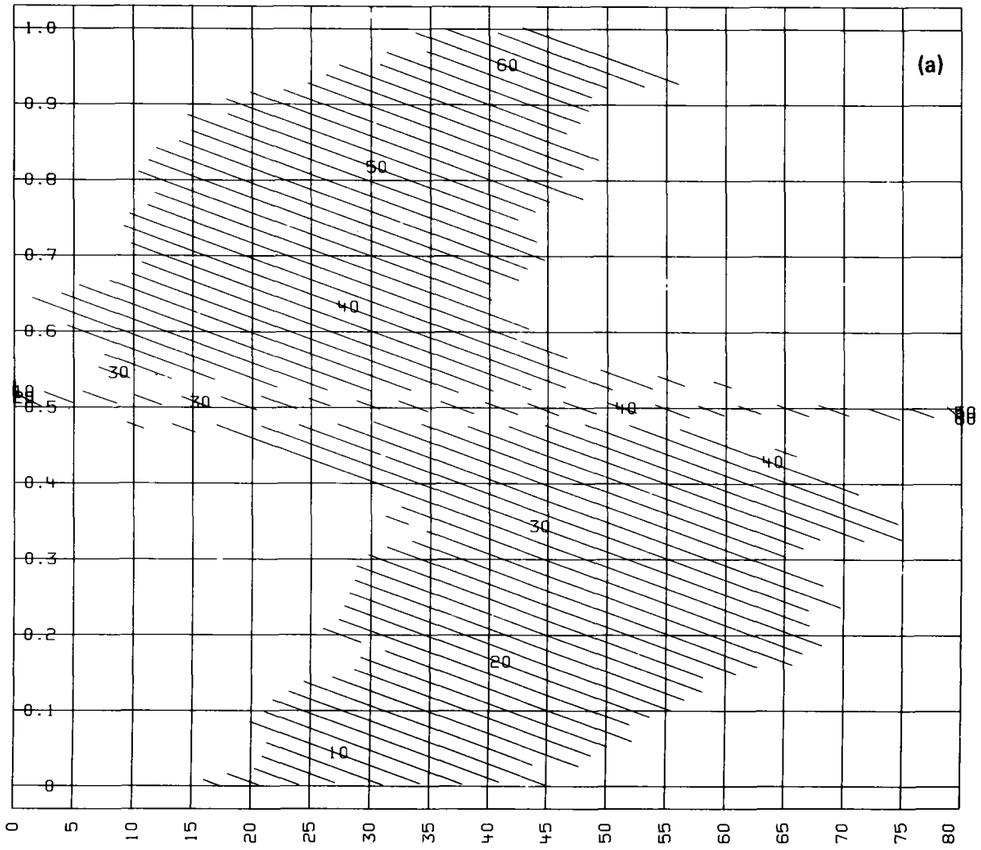

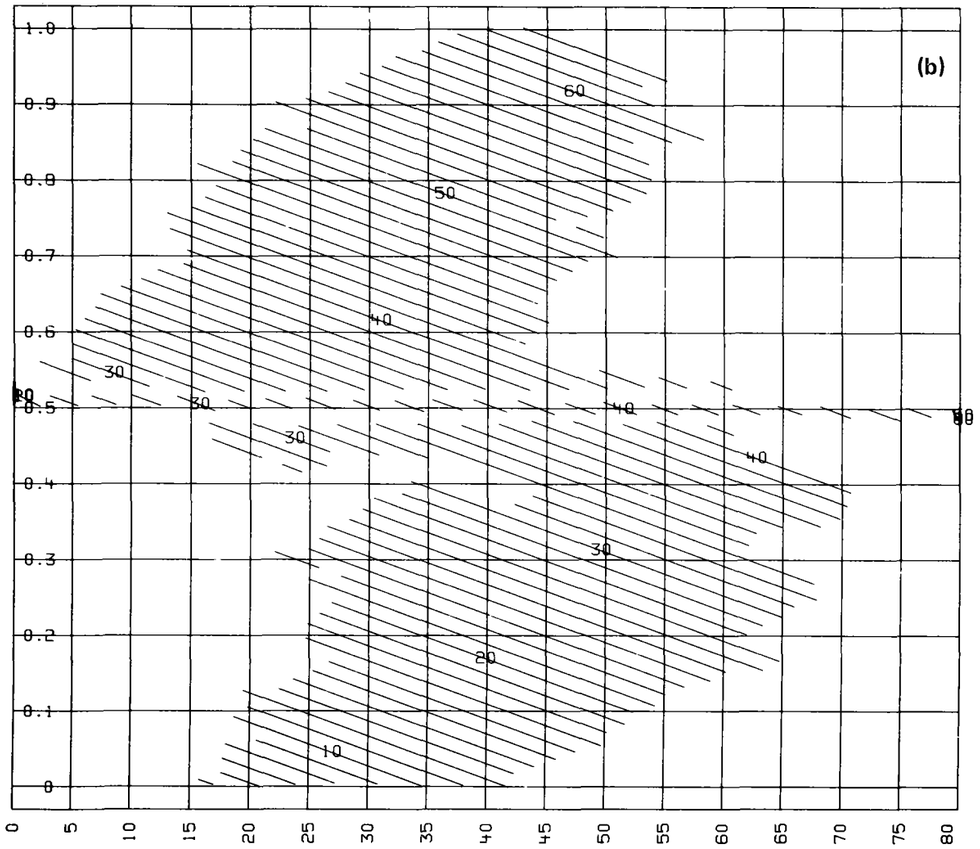

Figure 18. Acceptance window plots for the crudely adjusted test collector. Angle α in mrad, measured from an arbitrary zero. There is fairly complete coverage between the 35 and 40 mrad grid lines. Figures (a) through (d) refer to the Q1 through Q4 cross sections, respectively.

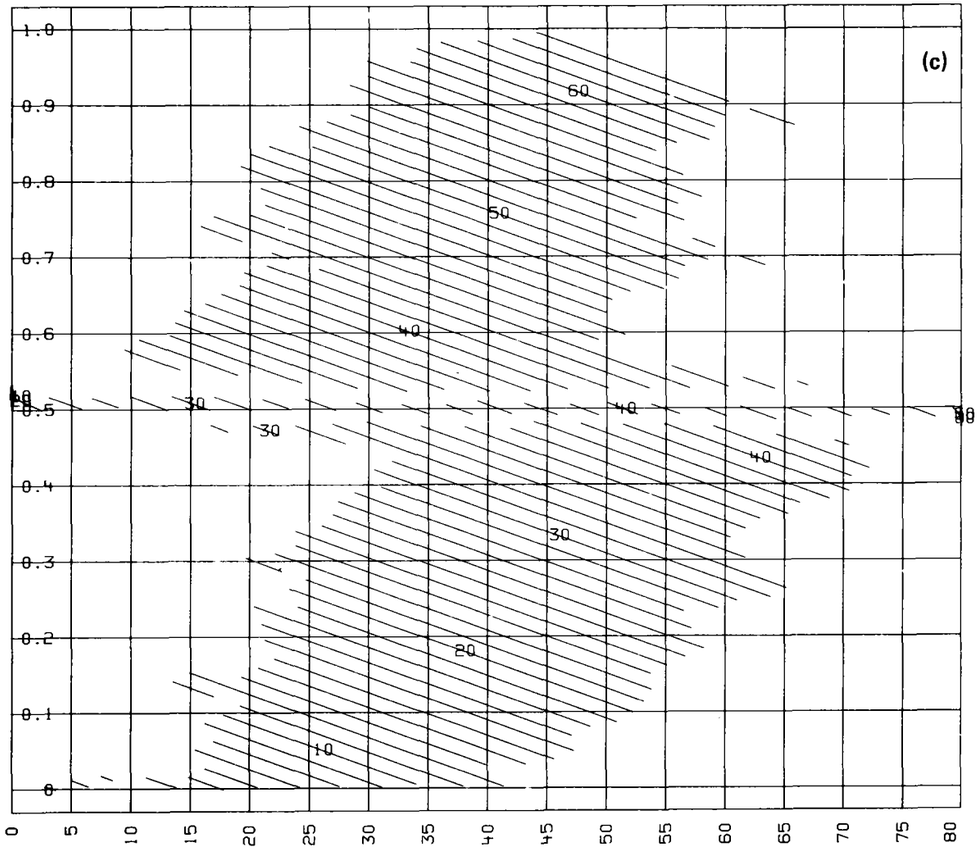

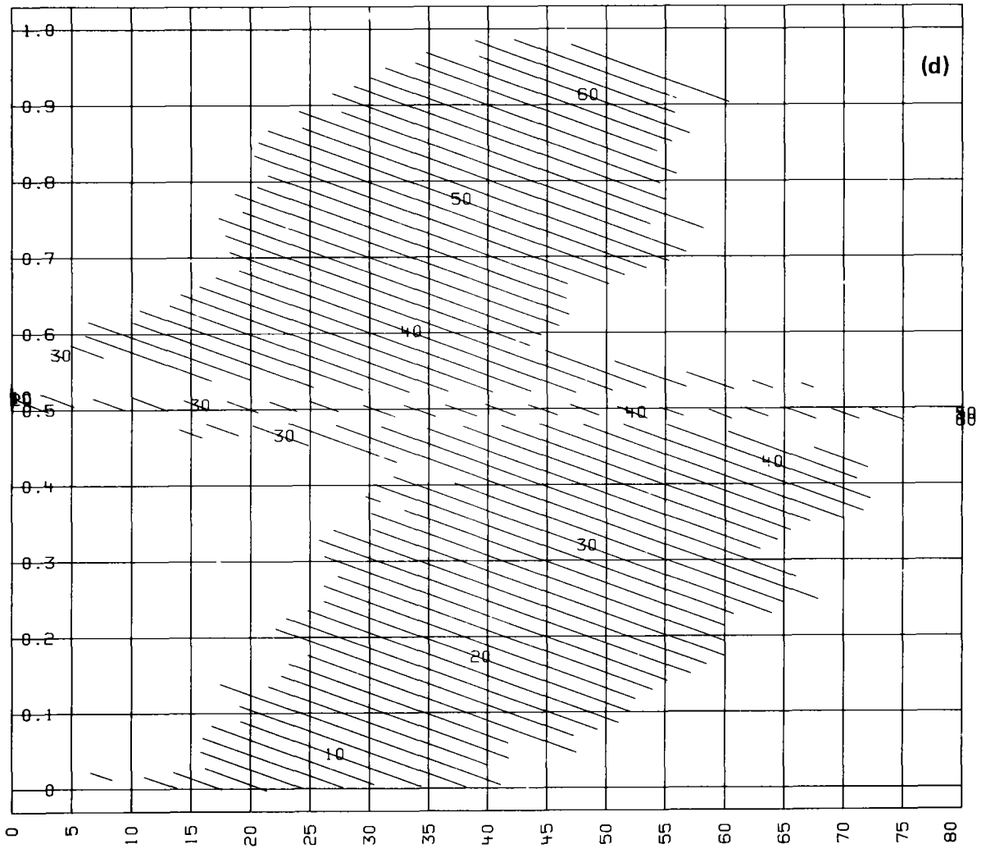

Figure 18. (Continued).

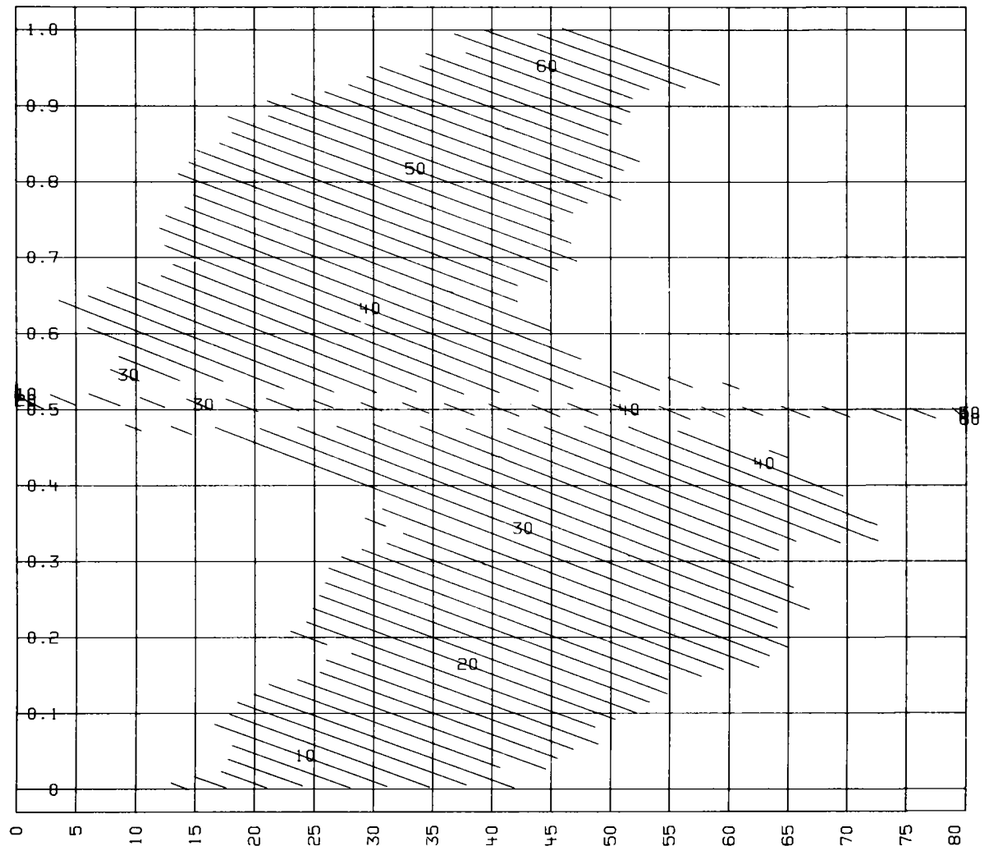

Figure 19. In this case, moving the receiver pipe outward rather than correcting the S-shape, has caused a shift of the window endpoints away from "center."

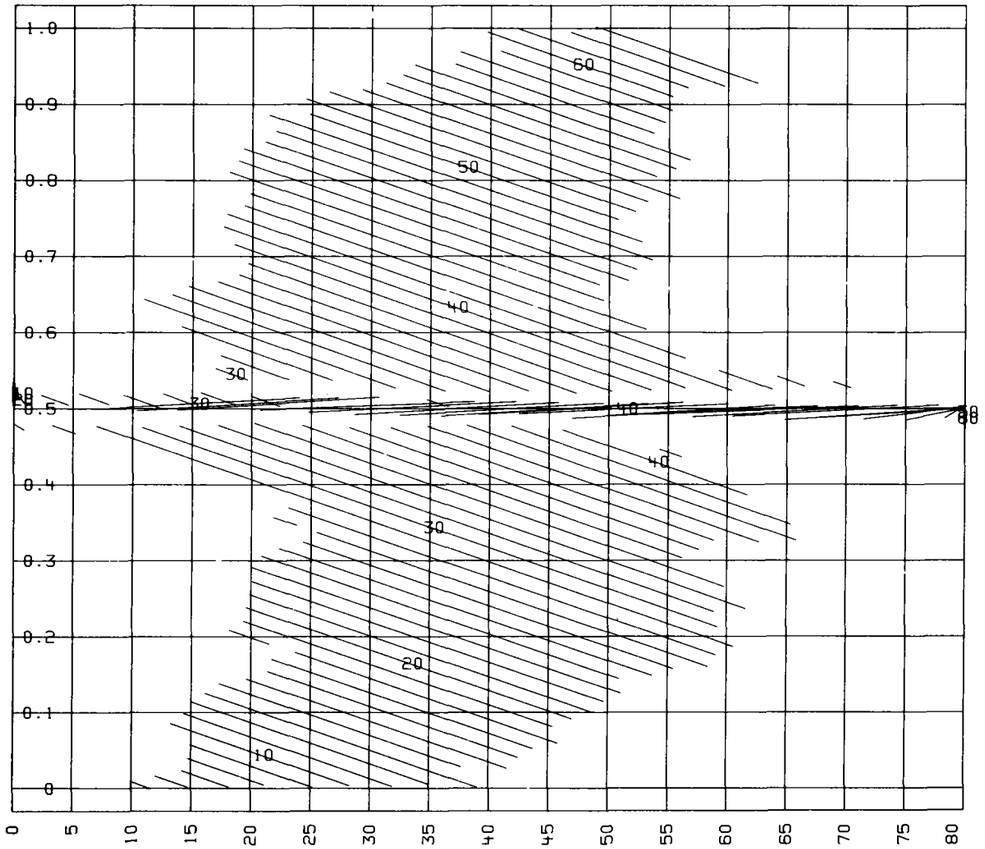

Figure 20. Rotating the mirror halves outward helps to align the center portions of the two window halves.

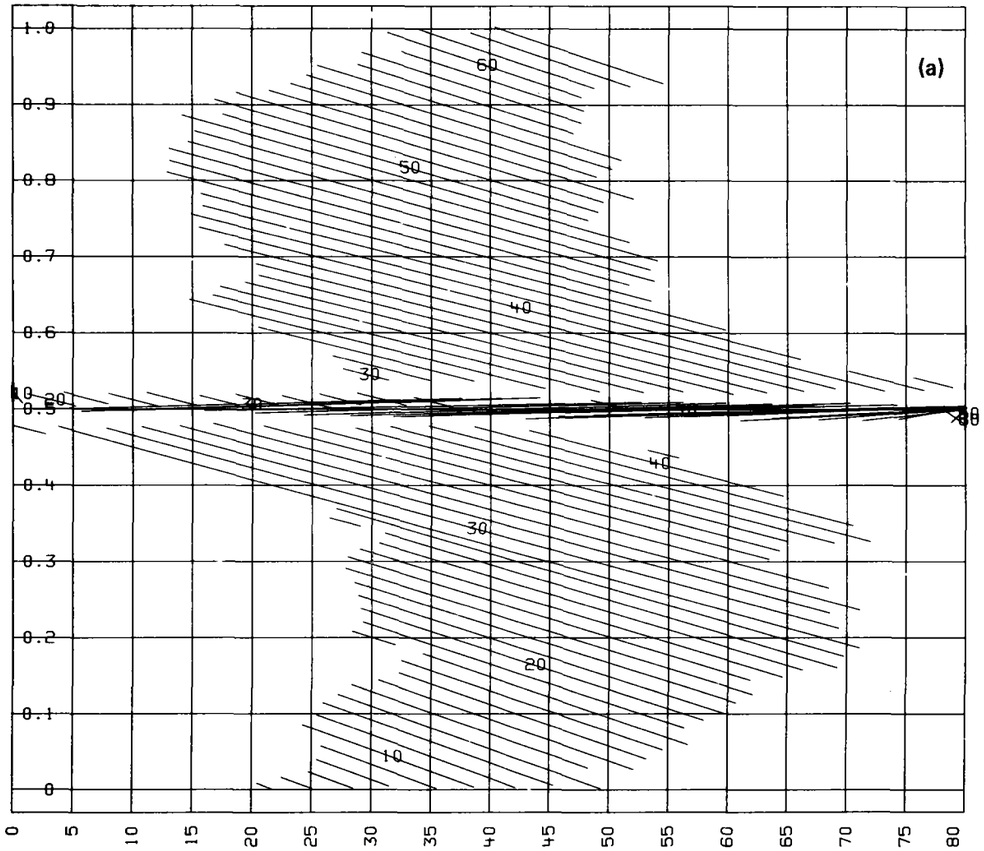

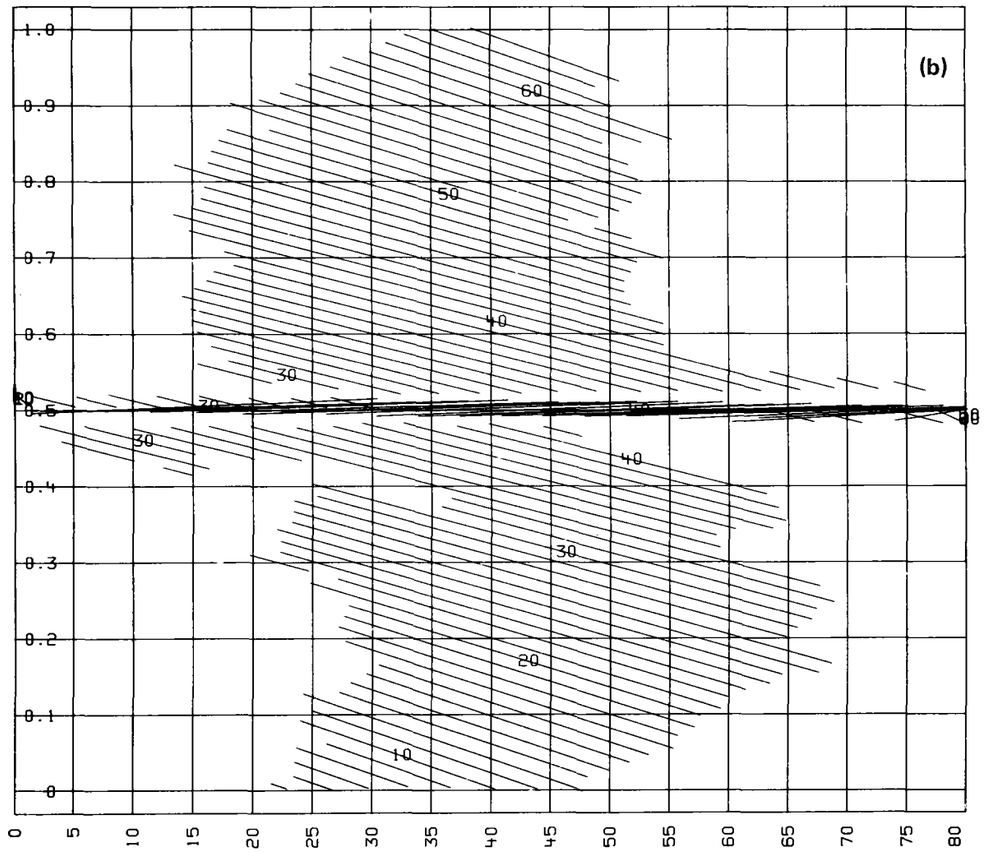

Figure 21. These predicted acceptance windows are based on the observations plotted in Fig. 18 and processed with the collector adjustments summarized in Table 1. Figures (a) through (d) refer to the Q1 through Q4 cross sections, respectively.

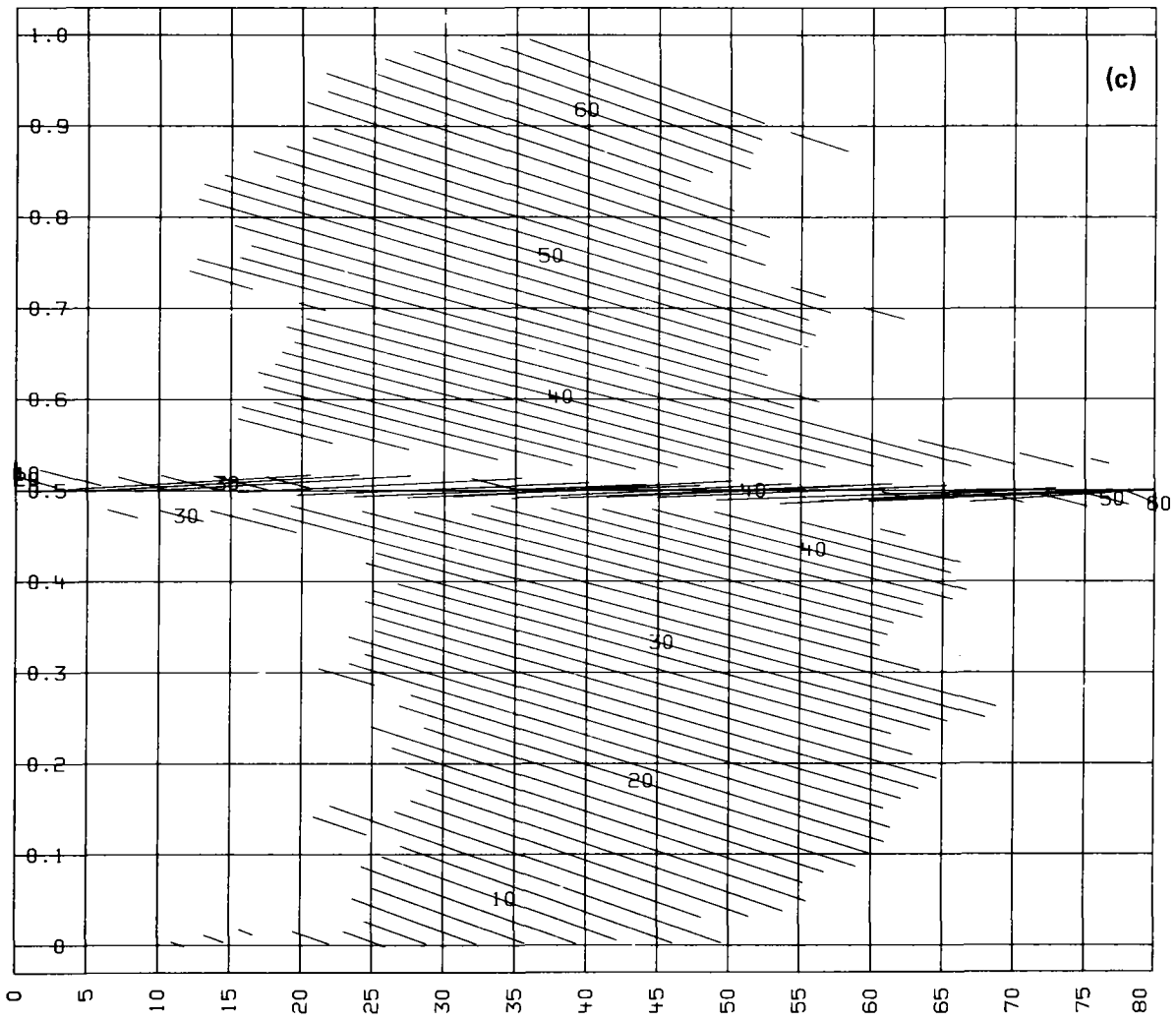

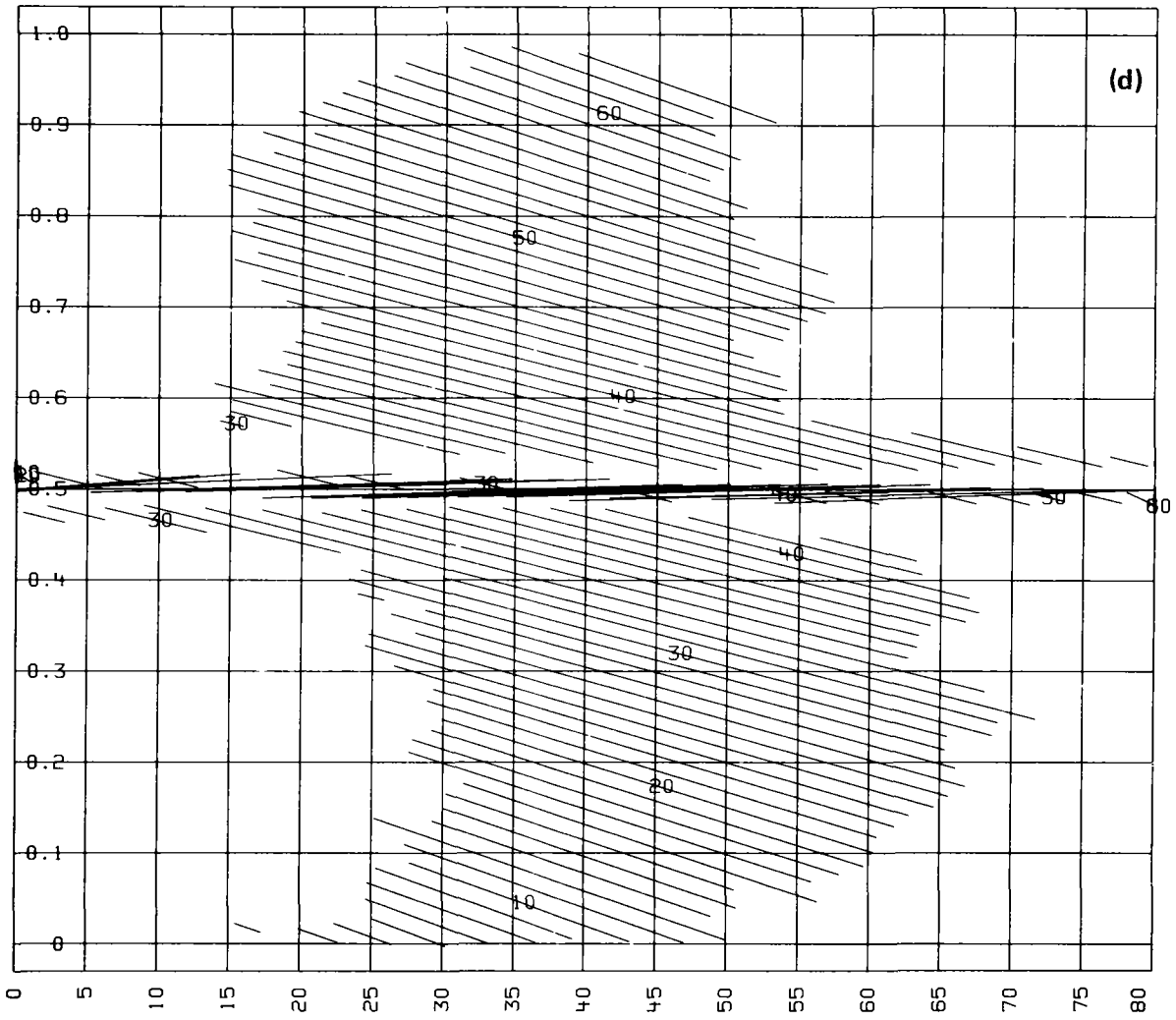

Table 21. (Continued).

Table 1. Adjustments necessary to achieve widest possible 100% acceptance bands.

Cross section	Q1	Q2	Q3	Q4
Move pipe outward (%)	2.5	2.5	2.5	3
Move pipe downward (%)	0.5	0	0	0
Rotate upper mirror outward (mrad)	10	9	6	9
Rotate lower mirror outward (mrad)	10	8	6	8

100% acceptance band which is 13 to 18 mrad wide. The manufacturer's data shows a 914-mm (36-in.) focal length. Our adjustments put it at 945 mm (37.2 in.) for the best collection. Finally, as a proof that this process works, we made adjustments to the collector and retested it. The actual adjustments made were based on a preliminary analysis of the above data.

Figure 22 illustrates the predicted acceptance window based on the data from the first test processed with the actual collector modifications made, while Fig. 23 is a plot of unadjusted data from the second test. The two match very well, except for a shift on the relative angle scale, where a slightly different arbitrary zero point is selected. Visual observations with binoculars from 500 m distance and with very slow manual rotation of the collector verified 100% acceptance for at least 10 mrad.

SCHEME B: MOVING OBSERVER AT EXTREME DISTANCE

In this version of the test, the observer views the field of collectors from a moving aircraft. A 16 or 35 mm motion picture camera is suggested for recording the data. Because of the vibration of the aircraft, it is necessary to use shutter speeds $\geq$ 1/125 s.

In spite of the apparent complication associated with hiring an aircraft and pilot for a flyby or two, the potential advantages of this type of test are substantial when the number of collectors and area to be tested are large.

The first advantage is that it is practical to view many collectors, perhaps a whole field at once. This can save observation and set-up time. Second, from a distance >100 $\times$ w it becomes much less necessary to correct

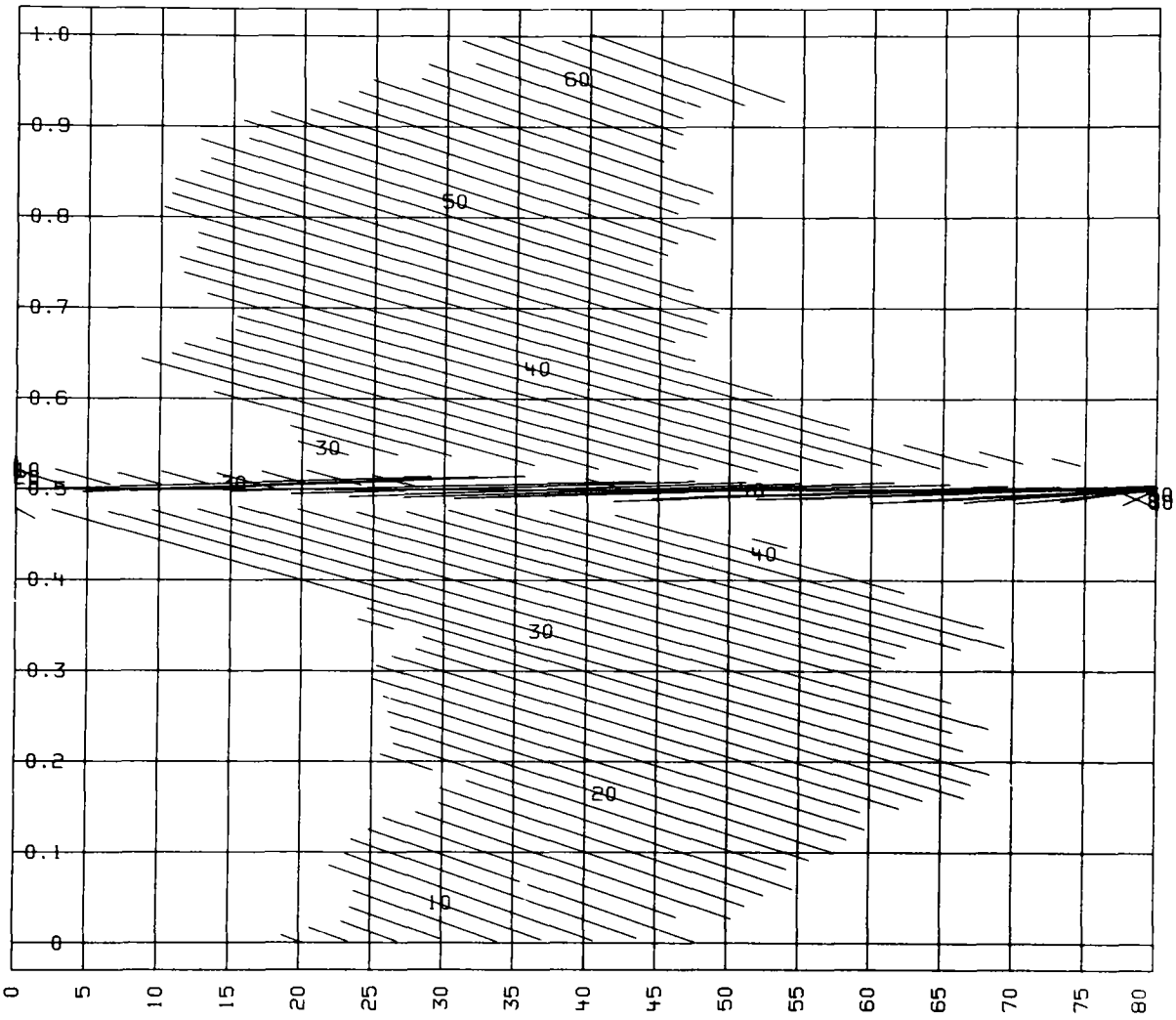

Figure 22. This acceptance window for the Q1 cross section is the predicted result of actual collector adjustments.

the observations for parallax angle as described previously. The observer distance need not be accurately measured. This eliminates one instrument from the collection, and plotting the data is simplified. Third, the observations are made while the collectors are in normal operation. There is no system downtime, and there is a minimum of interference with plant operations and maintenance personnel.

The fourth advantage is that the alignment of the sun-seeking mechanism with the true optical axis can be checked along with the receiver/reflector geometry. From this distance and with this relatively large field of view, it would be difficult to use the red and yellow checkerboard protractor. Instead, one could use the shadow of the plane to determine the off-axis angle. A flight path should be chosen roughly perpendicular to the trough

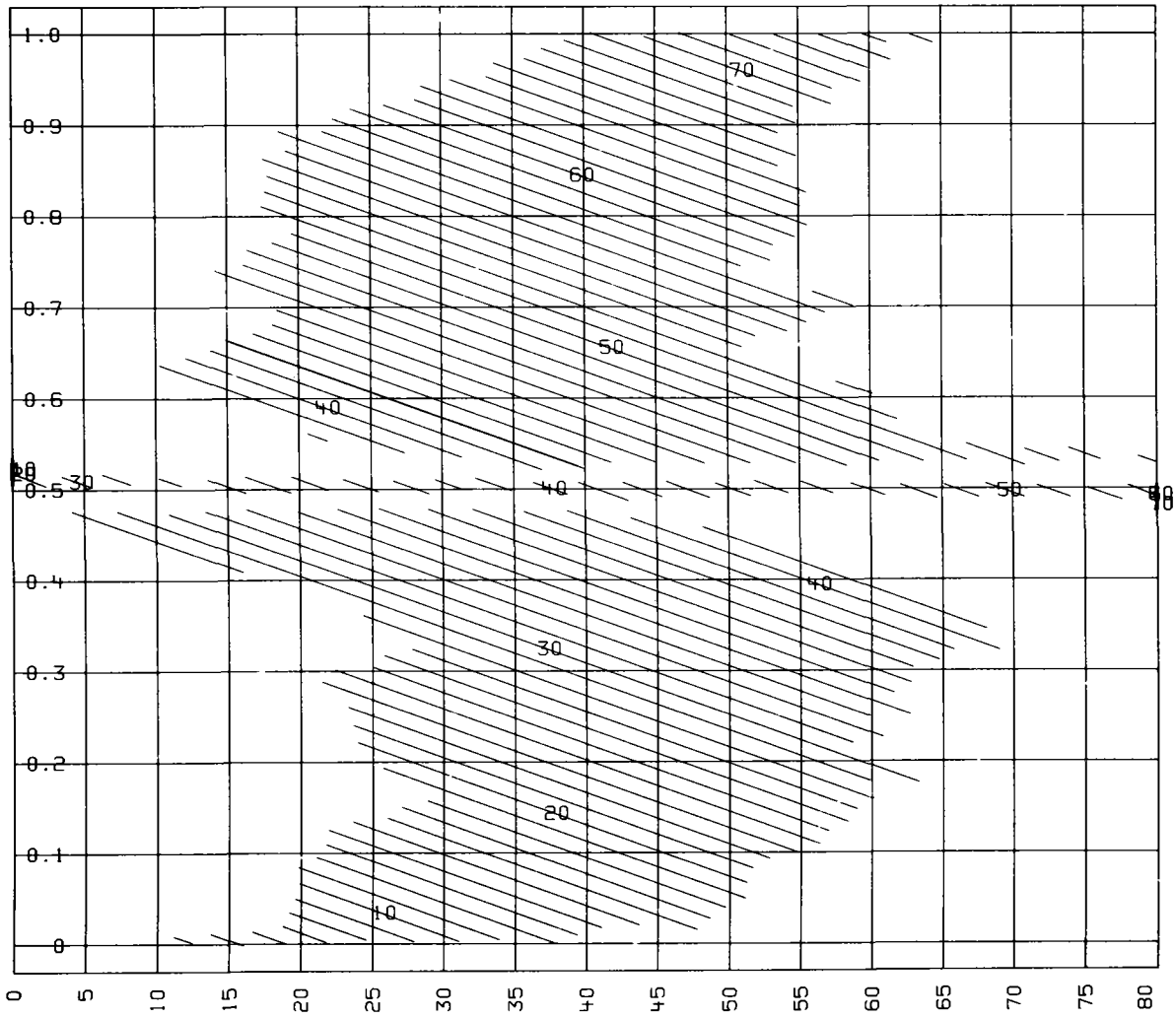

Figure 23. This acceptance window for the Q1 cross section is plotted from a retest of the collector after adjustment.

axis, and the shadow of the plane should cross the collector field. Again, this should be done at a time when the sun will not appear in the reflected background; otherwise, the reflected circumsolar light will wash out the photo (e.g., before 10 am and after 2 pm for East-West troughs, between 1 am and 2 pm for North-South troughs). The altitude should not be too great or the shadow will not be recognizable.

When everything is adjusted perfectly, the sequence of pictures should resemble the sketch in Fig. 24. At first, only the sky can be seen reflected in the array of mirrors. As the shadow approaches each row of collectors, the image of the receiver should appear along the trough's central axis and grow to fill the aperture. The aperture should stay filled until the

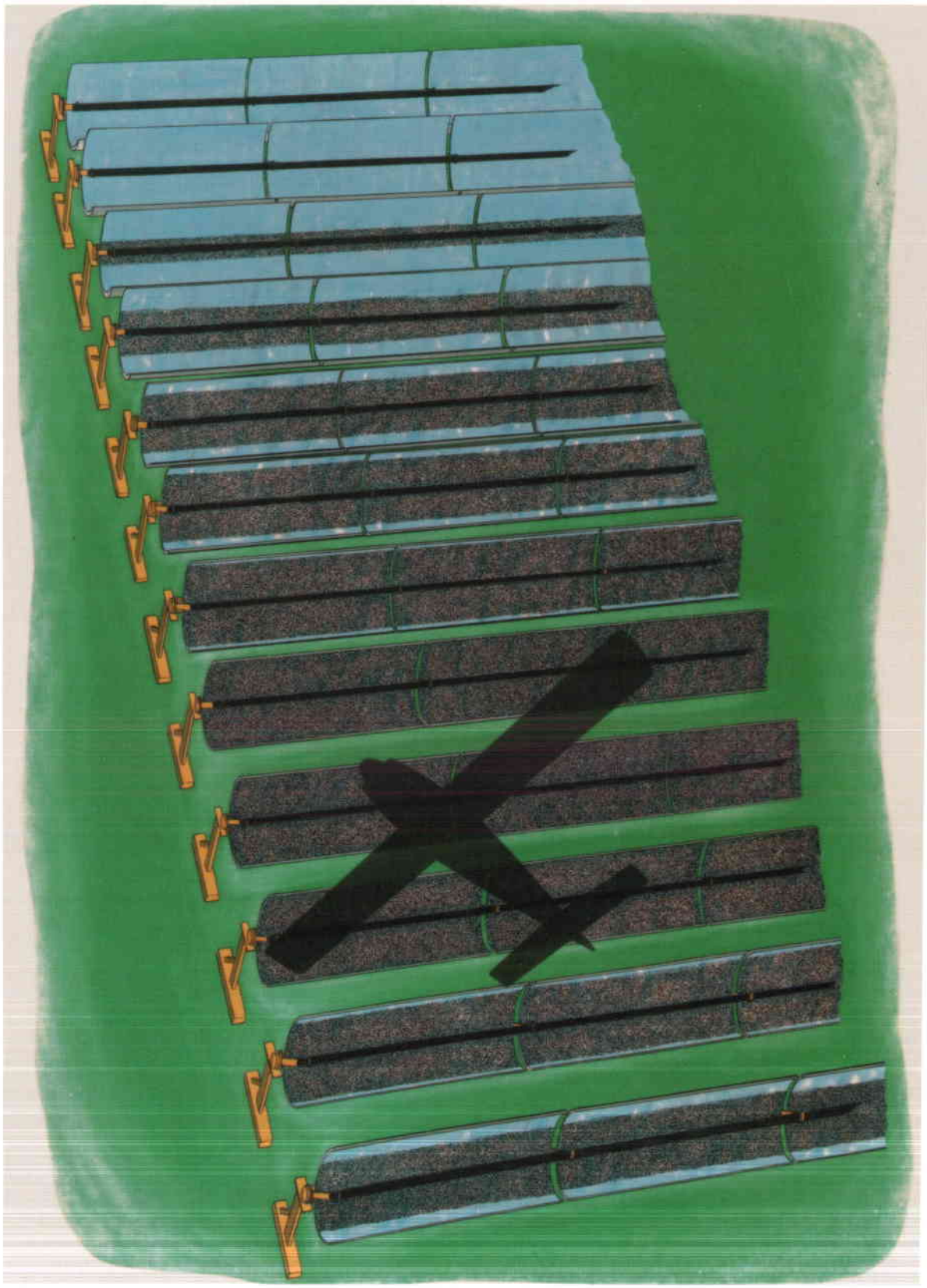

Figure 24. When a collector field is viewed from the air, the receiver-pipe image should completely fill the trough directly inline with the observer's shadow; if not, either the collector is misshapen or the tracker is misaligned.

photographer's shadow has passed. Then the pipe image should diminish again toward the center until it disappears.

The position and movements of the image in an actual collector can be compared directly to the curves derived earlier that define specific faults. From a performance standpoint, the only concern is that each trough aperture should be filled completely by the receiver image while the distant observer's shadow is crossing it. As long as this condition is met, adjustments to the collector to improve its configuration are not likely to improve its performance immediately, although future drift problems may be avoided. If the totally filled band is not centered on the frame where the observer's shadow falls directly on the center of the trough, the sun seeker is not pointed in the best direction.

Again, this version of the method allows testing of large arrays with a minimum of field-technician time and the least interference to normal plant operation. Sunseeker alignment is checked simultaneously and, whereas the longer viewing distance and larger field of view may make exact quantitative collector fault identification more difficult, qualitative analysis of the film is extremely easy and fast. Any questionable collector modules can be subjected to the more quantitative test.

SCHEME C: MOVING OBSERVER AT CLOSE RANGE

This scheme is the least quantitative of the three given here, but it also requires the least hardware and data reduction. Like the long range version, the observations are made while the collector is in operation. A camera is used at close range to take pictures of its own shadow cast on various spots on the reflector. If the collector and tracker are adjusted adequately, the shadow should always be framed by an image of the receiver.

We attempted this test once, with some success, but it was not as easy as it seems. One problem is getting complete coverage of the collector. For example, we could not reach the far upper side of the collector from a platform on top of the pipe rack of a pickup truck. Perhaps having a wide angle lens and a long pole on which to mount the camera would help.

Additionally, although the photographer saw the shadow during the filming it is very difficult to detect on the photos (see Fig. 25a). Perhaps using a

separate pointer or a white sheet on which to cast part of the shadow would help (see Fig. 25b).

Our test collector had no sunseeker; therefore, the few photos we took were immaterial. A tracking mechanism must be in operation for the test to be valid.

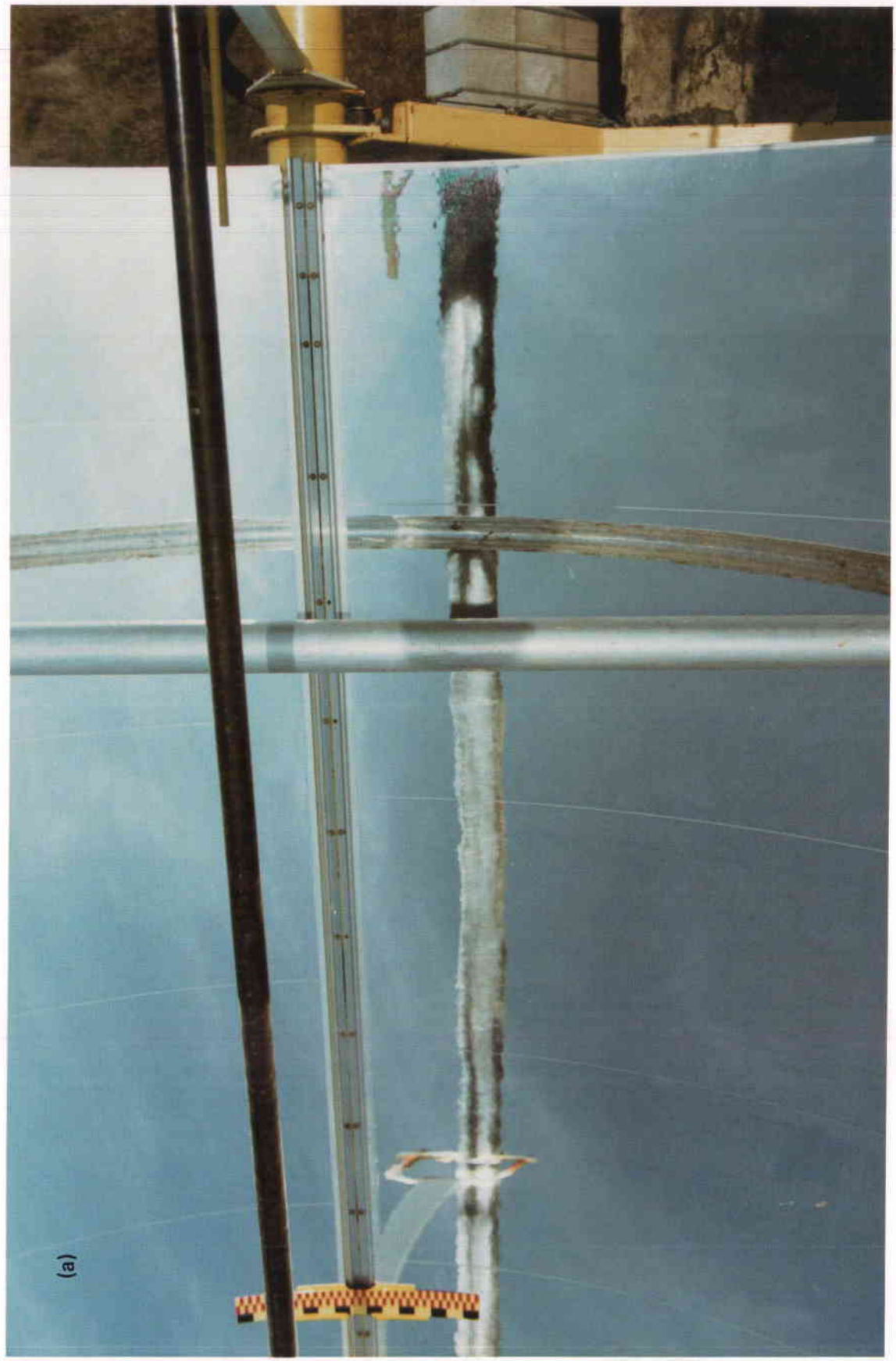
(a)

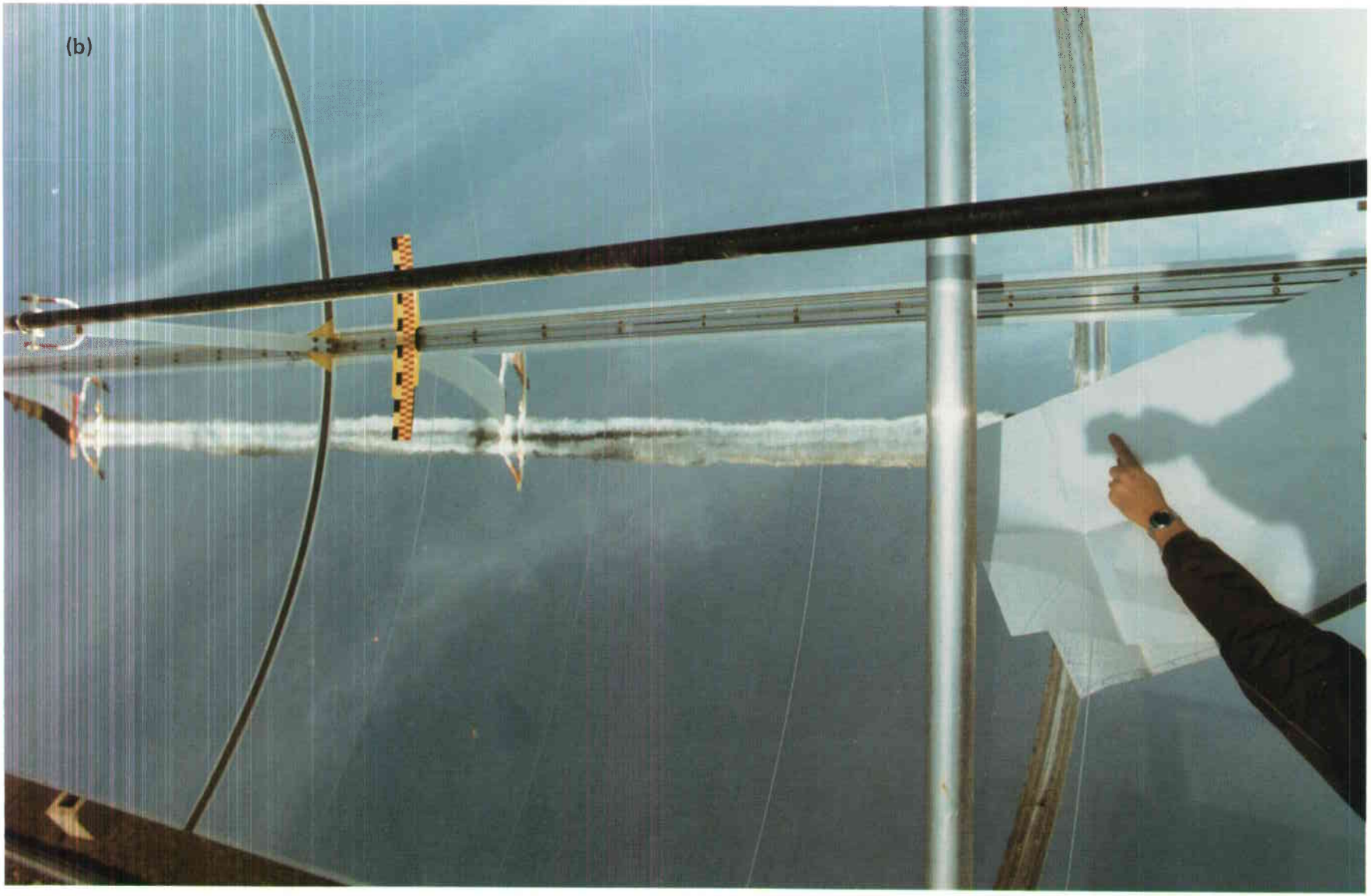

Figure 25. When an operating collector field is viewed at close range, the observer's shadow (camera) should appear to be on the receiver image at all times.

CONCLUSION

Distant observer techniques promise to be valuable tools for testing the optical conformation of large parabolic trough systems. The amount of precision testing hardware required in the field is much less than competing analytical methods. Interference with normal plant operation is exceedingly short or nonexistent. Adequate and inadequate collector modules can be identified quickly. Quantitative analysis of the data indicates which adjustments can be made to receiver pipe location, mirror facet angle, and tracking mechanism alignment to alleviate manufacturing errors. No competing method lends itself to this type of remedy.

All versions of the test method take relatively little time to make and record the field observations. Shadow/image versions (e.g., schemes B and C in the report) require very little analysis to verify whether an optical conformation is acceptable or unacceptable. Quantitative analysis will be a little more involved, as described.

Non-shadow versions (e.g., scheme A in the report) do not test tracker-alignment. From intermediate and short distances the observation data must be adjusted for parallax. With standard movie or still-camera recordings, this can be an involved task. We have proposed to modify a strip camera (e.g., photo-finish cameras which give a cross-section-vs-time picture) to directly produce a single print showing image position vs axis angle (i.e., the acceptance plot). This improvement would remove all the tedious data reduction necessary now and turn this already superior test method into an irreplaceable tool for the solar industry.

ACKNOWLEDGMENT

The author thanks David Dixon of Lawrence Livermore National Laboratory's Technical Photography Group for his expert assistance in the preparation of this report.

LR

U.S. Government Printing Office: 1982/8- 590-473

Technical Information Department · Lawrence Livermore National Laboratory
University of California · Livermore, California 94550

First Class Mail

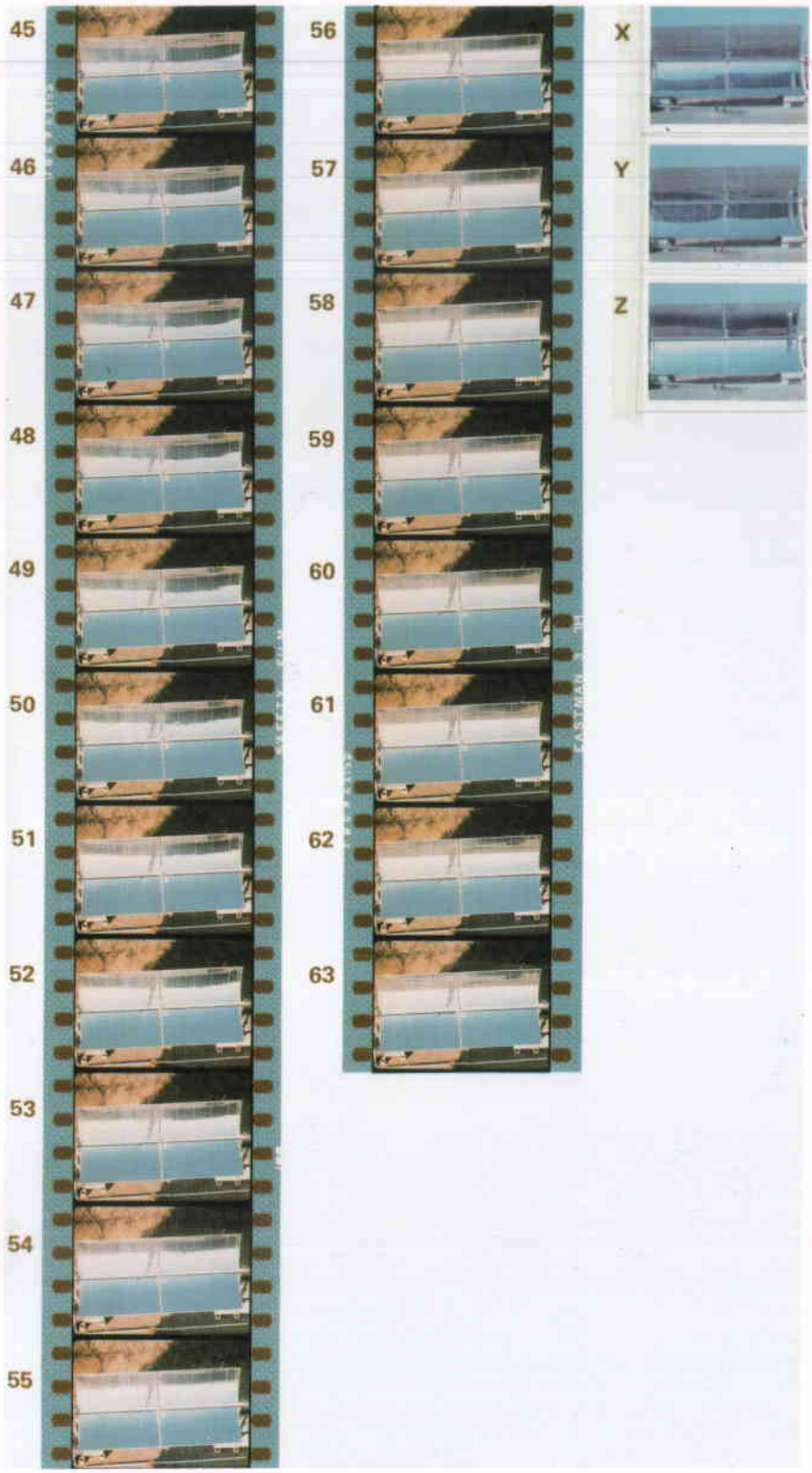
45
46
47
48
49
50
51
52
53
54
55
56
57
58
59
60
61
62
63
X
Y
Z